HOW DOES FINE-TUNED FOUNDATION MODELS HELP FOR LONG-TAILED DATA

Anonymous authors
Paper under double-blind review

ABSTRACT

Deep long-tail learning is a challenging visual recognition problem that trains models on long-tailed distributed datasets. In the last decade, a large number of methods have been proposed to solve the problems caused by imbalanced data. Many methods have been proven useful in learning a deep model from scratch, such as ResNet or ResNeXt, but they have not been validated as effective in fine-tuning the pre-trained foundation models, such as CLIP or ViT. If users inappropriately apply these long-tail learning methods, it may result in worse accuracy than expected. However, there is no scientific guideline for these methods in the existing literature. In this paper, we first collect the widely used methods of existing long-tail learning and then conduct extensive and systematic experiments to provide a guideline for the accurate use of these methods in fine-tuning foundation models. Furthermore, we observe that the current comparison protocol ignores the influence of training cost and hyperparameter selection, which may potentially lead to unfair comparisons and biased results. Motivated by our empirical studies, we propose a unified fine-tuning framework for long-tailed recognition. Experimental results demonstrate that the proposed framework outperforms existing methods on multiple long-tailed datasets, including ImageNet-LT, Places-LT, CIFAR100-LT, and iNaturalist 2018.

1 INTRODUCTION

Deep neural networks have achieved great success in a variety of computer vision tasks, such as image recognition (Voulodimos et al., 2018; Krizhevsky et al., 2012), object detection (Zhao et al., 2019; Zou et al., 2023), etc. These achievements are attributed to the availability of large-scale datasets (Deng et al., 2009; Zhou et al., 2017; Krizhevsky, 2009) and the elaborately designed models (He et al., 2016; Dosovitskiy et al., 2021). However, in the real world, the natural data typically exhibits a long-tailed distribution (Liu et al., 2019; Cao et al., 2019; Kang et al., 2020; Yuan et al., 2021a; Yan et al., 2023; Xu et al., 2023a), where a small number of head classes have the majority of samples, and a large number of tail classes have only a few samples. Such extreme class imbalance poses severe challenges to the training of deep neural networks. The reason lies in that the models are prone to making predictions biased towards the head classes, leading to poor performance on tail classes, thereby decreasing the overall prediction performance (Tan et al., 2020; Zhang et al., 2023).

To solve the long-tail problem, many methods have been proposed in recent years. For example, re-weighting methods (Wu et al., 2020; Khan et al., 2019; Cui et al., 2019) aim to adjust the training loss for each class by multiplying it with a different weight; re-sampling methods (Chawla et al., 2002; Liu et al., 2008; Shi et al., 2023) aim to adjust the number of samples for each class in each sample batch to rebalance the classes; ensemble learning methods (Zhou et al., 2020; Wang et al., 2021b) aim to combine multiple exports to reduce the bias of the model towards the head classes. These existing methods have made significant progress in improving classification accuracy, but the experimental results of these methods are obtained from models trained from scratch, with limited research on fine-tuning pre-trained foundation models.

Recently, some works study long-tail learning with foundation models instead of training from scratch, such as BALLAD (Ma et al., 2021), VL-LTR (Tian et al., 2022), LPT (Dong et al., 2023), LIFT (Shi et al., 2024), and RAC (Long et al., 2022). However, these studies are less comprehensive and lack a systematic investigation. BALLAD and VL-LTR focus on two-stage learning methods, while LPT and LIFT utilize rebalanced loss functions to mitigate the long-tail problem. On the other hand, BALLAD, VL-LTR, and RAC only apply the full fine-tuning setting, while LPT and LIFT focus solely on the parameter-efficient fine-tuning approaches. To the best of our knowledge, there has not been a systematic study on how to fine-tune foundation models under a long-tailed distribution.

In this paper, we delve into the commonly used methods in long-tail learning and apply them to fine-tune pre-trained CLIP (Radford et al., 2021) and ViT (Dosovitskiy et al., 2021), which are widely used in various visual tasks (Dehghani et al., 2023; Zhou et al., 2022; Yuan et al., 2021b; Wang et al., 2021a; Gao et al., 2024). We conduct extensive and systematic experiments to evaluate whether these methods are equally effective on foundation models as learning from scratch. We also analyze their training costs and hyperparameter selections. Finally, motivated by the results of our empirical studies, we integrate the optimal methods and propose a unified training framework. The proposed framework achieves better results than existing approaches on multiple long-tailed datasets, including ImageNet-LT (Liu et al., 2019), Places-LT (Sharma et al., 2021), CIFAR100-LT (Cao et al., 2019), and iNaturalist 2018 (Van Horn et al., 2018).

The main contributions of our work are as follows:

- We thoroughly explore the effectiveness of commonly used methods in long-tail learning when applied to foundation models to provide guidance for future research.
- We propose a unified fine-tuning framework by assembling optimal methods, which outperforms existing methods on multiple long-tailed datasets.
- We investigate training costs and hyperparameter selection in experiments to offer comprehensive recommendations for the use of these methods in practical settings.

2 Related Work

Long-Tail Learning There are several methods being proposed to address the long-tail problem (Liu et al., 2019; Cao et al., 2019; Cui et al., 2019; Kang et al., 2020; Zhou et al., 2020; Zhong et al., 2021; Yang et al., 2022; Zhang et al., 2023), which can be divided into three categories (Zhang et al., 2023): 1) Class re-balancing aims to enhance the model's ability to recognize minority classes by rebalancing the sample proportions across different classes, including re-sampling (Chawla et al., 2002; Liu et al., 2008; Shi et al., 2023), class-sensitive re-weighting (Wu et al., 2020; Khan et al., 2019; Cui et al., 2019), and logit adjustment (Menon et al., 2021; Zhang et al., 2021a; Hong et al., 2021). 2) Information augmentation aims to improve model performance on long-tailed data by incorporating additional information during model training, including transfer learning (Cui et al., 2018; Xiang et al., 2020) and data augmentation (Shorten & Khoshgoftaar, 2019; Zhong et al., 2021). 3) Module improvement methods seek to address long-tail problems by improving network modules or representations, including classifier design (Wu et al., 2021; Liu et al., 2021a), contrastive learning (Kang et al., 2021; Zhu et al., 2022), and ensemble learning (Zhou et al., 2020; Wang et al., 2021b). However, these works only study how to train models from scratch and ignore the development of pre-trained foundation models. In this paper, we aim to further investigate the specific effects of the representative methods by applying them to the advanced foundation models.

Fine-Tuning Foundation Models The pre-trained foundation models have attracted widespread attention in recent years (Vaswani et al., 2017; Dosovitskiy et al., 2021; Radford et al., 2021; Touvron et al., 2021; Liu et al., 2021b). These models are pre-trained on web-scale data to construct sophisticated features and transferred to various downstream tasks, such as image classification (Yuan et al., 2021a), object detection (Yan et al., 2023), and semantic segmentation (Xu et al., 2023a). Moreover, the adaptation to downstream tasks can be further improved by applying extra data to fine-tune the foundation model (Dosovitskiy et al., 2021; Zhou et al., 2022). There are two fine-tuning approaches: full fine-tuning (Kumar et al., 2022) and parameter-efficient fine-tuning (Zaken et al., 2022; Jia et al., 2022; Chen et al., 2022), where the latter is regarded as a typical efficient mode by introducing only a few learnable parameters. However, these methods mainly utilize the balanced data for fine-tuning, which may yield unsatisfactory results when directly applied to the long-tailed datasets (Shi et al., 2024). Although some works have been proposed to mitigate this issue (Ma et al., 2021; Tian et al., 2022; Dong et al., 2023; Zhang et al., 2021b), no research has systematically studied the impact of long-tail learning algorithms on foundation models. For the first time, we explore the reasonable application of long-tail learning methods on foundation models to provide a guideline for future applications.

3 Methods Gallery

We commence by introducing the Problem Definition, then categorize classical long-tail learning methodologies into 7 distinct groups: 1) Re-sampling, 2) Data Augmentation, 3) Class-sensitive Loss, 4) Balanced Classifier, 5) Knowledge Distillation, 6) Ensemble Learning, and 7) Other tricks. For each group, we first revisit relevant methods and then compare experimental performance. To ensure the reliability of our investigation, we experiment under different scenarios, including different foundation models (CLIP and ViT) and different fine-tuning paradigms (FFT and PEFT). Comprehensive details regarding the datasets and implementation settings are provided in Appendix Section A. Due to the page limit, the knowledge distillation method is introduced in Appendix Section B, and the ensemble learning method is presented in Appendix Section C.

3.1 Problem Definition

Long-tailed recognition aims to learn deep classification models from training datasets characterized by a long-tailed class distribution, where a small number of classes contain a large number of samples, while the majority of classes have only a few samples. Formally, we denote the long-tailed datasets with N samples as $D = \{x_i, y_i\}_{i=1}^{N}$. Besides, we denote n_i as the sample frequency of class i $(1 \leq i \leq K)$, then we have $N = \sum_{i=1}^{K} n_i$. In long-tail learning, the class frequencies are arranged in a descending order (Kang et al., 2020), i.e., if $1 \leq i < j \leq K$, then $n_i \geq n_j$. The imbalance ratio is defined as $r = \frac{n_1}{n_K}$, representing the ratio between the class with the largest number of images and the class with the smallest number of images, which can be used to describe the severity of the long-tailed distribution. In practice, r formulates a large number, which indicates that $n_1 \gg n_K$ in a long-tailed dataset. The goal of long-tail learning is to learn a model M from the imbalanced data D so that M can attain optimal predictions on test data.

3.2 Re-sampling

Due to the intrinsic data imbalance in the long-tailed data, conventional sampling methods result in more head-class samples than tail-class samples in each training batch (Kang et al., 2020; 2021; Zhu et al., 2022). Re-sampling tackles this issue by adjusting the sample distribution of each class within the training data.

Re-sampling Methods We investigate several classic and widely used re-sampling methods.

- Random Over-Sampling (ROS) (Buda et al., 2018) balances the data distribution by duplicating samples from the tail classes to increase their proportion in training data to achieve a more balanced sample distribution between head classes and tail classes.
- Random Under-Sampling (RUS) (More, 2016) aims to balance the data distribution by reducing the number of samples from the head classes to make their sample frequencies closer to those of the tail classes.
- Equalized re-sampling (EQ) (Kang et al., 2020; Shi et al., 2023) dynamically applies over-sampling or under-sampling to different classes by ensuring the total size of the dataset is unchanged. In this case, it obtains a balanced dataset without adding more training overhead.
- Square-root sampling (Kang et al., 2020) addresses limitations of balanced re-sampling—excessive discarding of head-class samples and redundant duplication of tail-class samples. This approach samples class j with probability $p_j = \frac{n_j^q}{\sum_{i=1}^{K} n_i^q}$ (n_i = class sample count). Setting $q = \frac{1}{2}$, it reduces head-class sampling frequency while preventing over-balancing between head and tail classes.

Experimental Result Table 1 shows the results of using different re-sampling methods on CIFAR100-LT and Places-LT datasets. For more detailed results, please refer to Appendix section D.1

Table 1: Accuracy of re-sampling methods. "Baseline" represents no resampling. **Bold** and underlined numbers represent the optimal and sub-optimal results, respectively; the same notations are applied to all tables below.

Datasets	CIFAR100-LT				Places-LT			
Backbone	CLIP		ViT		CLIP		ViT	
	FFT	PEFT	FFT	PEFT	FFT	PEFT	FFT	PEFT
Baseline	54.6	71.9	70.3	80.7	24.7	39.8	26.0	32.1
ROS	44.8	68.3	48.3	71.0	12.6	38.3	11.4	32.2
RUS	45.5	**77.4**	69.3	**87.0**	**42.3**	**50.8**	**41.2**	**45.3**
EQ	50.4	72.8	62.0	77.3	21.7	43.7	22.0	33.7
Square-root	**56.8**	76.4	**76.0**	84.4	37.1	47.5	32.6	39.7

Based on our experimental findings, these sampling methods consistently perform better under the PEFT setting than under the FFT setting. RUS and Square-root sampling are proven to be more effective strategies, which can significantly enhance performance by more than 5%. In contrast, ROS exhibits significant performance deterioration, which is due to the severe overfitting issue. The performance of EQ is between RUS and ROS.

Given that the model is already pre-trained, these results appear to be justifiable: a minimal amount of data is sufficient to fine-tune the model and improve its performance on long-tailed datasets. We conduct an additional experiment to verify this point. Specifically, we compare the balanced dataset obtained through the RUS with 2, 5, and 10 times larger variants. Table 2 reports the results on the CLIP-ViT-B/16 PEFT setting, showcasing that RUS performs better, particularly on tail classes. As the data amount grows larger, though the head-class performance slowly increases, the tail-class performance exhibits significant declines.

We evaluated the models with two RUS and RUSx10 to enable a deeper mechanistic analysis. We extract the features of **tail-class** test data from CIFAR100-IR100 using these two models and visualize the results using t-SNE, as shown in Figure 1a 1b. The ellipse is constructed using the eigenvectors and eigenvalues of the covariance matrix, derived from the data's mean and covariance, which define its orientation, major and minor axes, and center.

Figure 1: t-SNE visualization and classifier weight norms for RUS and RUSx10.

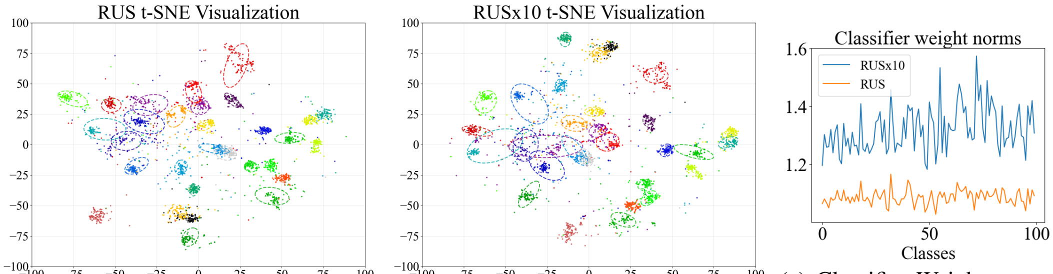

(a) t-SNE visualization for RUS

(b) t-SNE visualization for RUSx10

(c) Classifier Weight norms for RUS and RUSx10.

It can be observed that the ellipses in the t-SNE plot for RUS exhibit less overlap. This indicates more distinct decision boundaries for the tail classes, leading to better tail classification performance. Additionally, the weight norms of the model's classifier are presented in Figure 1c. RUS clearly demonstrates a more balanced distribution across all classes.

Furthermore, in terms of the training cost, the samples produced by RUS and Square-root sampling are significantly fewer, nearly 100 times less than those generated by ROS (the number varying with the dataset). Therefore, the training time cost is substantially lower than that of ROS and EQ under the same setting. Considering the above factors, using RUS or Square-root sampling is more practicable for fine-tuning foundation models with long-tailed datasets.

3.3 Data Augmentation

Data augmentation (Shorten & Khoshgoftaar, 2019) aims to increase data diversity by applying predefined transformations, thereby improving model generalization, especially in scenarios where the available data is limited.

Table 2: RUSxN indicates that the training dataset size is N times that of the RUS-sampled dataset, with each class containing N times the data as in RUS; "-" in the table means the corresponding experiment is not implemented due to the huge amount of data.

Datasets	CIFAR100-LT				Places-LT			
	Mean	Many	Med.	Few	Mean	Many	Med.	Few
RUS	**77.7**	82.0	80.0	**69.9**	**50.8**	49.6	52.2	**49.6**
RUSx2	77.5	85.3	**80.6**	64.6	50.6	50.5	**52.6**	46.1
RUSx5	75.6	87.2	79.7	57.4	49.1	51.5	51.4	39.2
RUSx10	73.4	**88.1**	77.8	50.7	47.7	**52.7**	48.9	33.9

Table 3: Accuracy of applying augmentation methods.

Datasets	CIFAR100-LT				Places-LT			
Backbone	CLIP		ViT		CLIP		ViT	
	FFT	PEFT	FFT	PEFT	FFT	PEFT	FFT	PEFT
No augmentation	48.7	71.9	71.1	**81.6**	23.7	39.8	25.7	31.7
ColorJitter	54.6	71.9	70.3	80.7	24.7	39.8	26.0	32.1
RandAugment	56.7	**72.1**	70.0	81.5	**25.4**	40.4	26.5	32.6
AutoAugment	**57.8**	70.7	**71.6**	81.3	24.9	**40.7**	**26.9**	**32.7**

Augmentation Methods In our paper, in addition to conventional image processing, we apply several common data augmentation techniques.

- ColorJitter is one of the most commonly used methods for color-based data augmentation in images. It applies random transformations within a specified range to the image's brightness, contrast, saturation, and hue.
- AutoAugment (Cubuk et al., 2019) creates a search space of strategies, each containing multiple sub-strategies. For each mini-batch image, one sub-strategy is randomly selected. Each includes two processing functions—like rotation, inversion, or shearing—with their probability and magnitude parameters.
- RandAugment (Cubuk et al., 2020) is a simplified version of AutoAugment. The core of RandAugment is to randomly select a set of predefined augmentation operations with equal probability and assign an intensity hyperparameter to each operation to transform the input images.

Experimental Results Table 3 shows the results of different augmentation methods on different datasets and settings. For more detailed results, please refer to Appendix section D.2.

Based on the experimental results, it can be concluded that solely applying data augmentation to long-tailed datasets can just slightly improve the performance of foundation models by less than 1%. Furthermore, when combined with other long-tail learning methods, data augmentation can not always gain benefits, which will be discussed in Section **The Ultimate Framework.**

Data augmentation introduces computational overhead during data preparation, consequently extending the total training duration. For example, our experiments demonstrate a 15% increase in end-to-end training time with RandAugment. In addition, we also research other impact of data augmentation on model training, as shown in Figure 2. We illustrate the convergence curves of training loss and accuracy for the ImageNet-LT dataset without augmentation and with AutoAugmentation. Based on the observations from the figures, it can be concluded that data augmentation slows down the convergence speed of the model. The reason why such kind of data augmentation without using external data faces difficulty in improving performance may be that foundation models have already seen various styles of images. Some recent studies have shown that introducing external data or knowledge for augmentation is effective (Long et al., 2022; Wang et al., 2024a), which may be an interesting direction in future research.

3.4 Class-sensitive Loss

Traditional deep learning methods typically employ the softmax cross-entropy loss function for training. However, this loss function often overlooks the issue of class imbalance among training data. We revisit some classic class-sensitive losses, which aim to rebalance the training loss for different classes to deal with the imbalance problem.

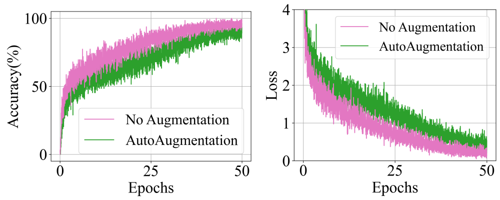

Figure 2: Convergence curves of training accuracy (left) and loss (right) on ImageNet-LT under CLIP-ViT-B/16 PEFT.

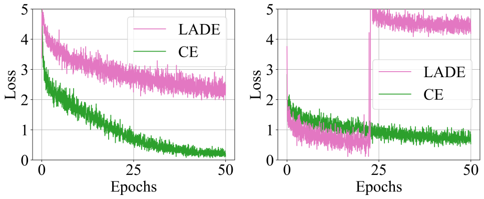

Figure 3: Training loss of LADE and CE on Places-LT under CLIP/B-16 FFT (left) and ViT/B-16 PEFT (right) setting

Table 4: Summary of losses. In the table, z is the predicted logits, p is the probability obtained by applying softmax to z, where z_y, p_y correspond to class y. $\pi_y = \frac{n_y}{N}$ represents the label frequency of the class y, where n_y represents the number of samples in class y, N is the total sample numbers.

Loss	Formulation	Hyperparam.	Loss	Formulation	Hyperparam.
CE	$-\log(p_y)$	-	G-RW	$-\frac{(1/\pi_y)^\rho}{\sum_j (1/\pi_j)^\rho} \log(p_y)$	ρ
Focal	$-(1-p_y)^\gamma \log(p_y)$	γ	BS	$-\log(\frac{\pi_y exp(z_y)}{\sum_j \pi_j exp(z_j)})$	-
LDAM	$-\log(\frac{exp(z_y - \Delta_y)}{\sum_j exp(z_j - \Delta_j)})$	s	LA	$-\log(\frac{exp(z_y + \mu \cdot \pi_y)}{\sum_j exp(z_j + \mu \cdot \pi_j)})$	μ
CB	$-\frac{1-\beta}{1-\beta^{n_y}} \log(p_y)$	β	LADE	$L_{BS} + \alpha L_{LADER}$	α, λ

Loss Functions We study common class-sensitive losses, which are listed in Table 4.

- **Focal Loss** (Lin et al., 2017): Modulates CE loss with γ to down-weight easy examples.
- **LDAM** (Cao et al., 2019): Assigns class-dependent margins (Δ) inversely proportional to class frequency.
- **CB Loss** (Cui et al., 2019): Reweights losses by the effective number of samples per class.
- **G-RW** (Zhang et al., 2021a): Generalizes re-weighting with scale parameter ρ.
- **Balanced Softmax** (Ren et al., 2020): Adjusts softmax weights by class sample sizes.
- **Logit-Adjusted** (Menon et al., 2021): Applies label-dependent offsets to logits based on class frequency.
- **LADE** (Hong et al., 2021): Calibrates outputs using test label distribution. Its regularizer L_{LADER} combines class priors π_j and normalization terms. $L_{LADER} = \sum_{j \in K} \pi_j L_{LADER_j}$, given $L_{LADER_j} = -\frac{1}{N_j} \sum_{i=1}^{N} \mathbf{1}_{y_i = j} \cdot \pi_j + Z + \sum_j \pi_j \lambda Z^2$, where $Z = \log(\frac{1}{N} \sum_{i=1}^{N} \frac{z_j}{K \pi_y})$.

Experimental Result We present the experimental result in Table 5. For more parameter settings and results, please refer to Appendix section D.3.

Table 5: Accuracy of applying class-sensitive losses.

Datasets	CIFAR100-LT				Places-LT			
Backbone	CLIP		ViT		CLIP		ViT	
	FFT	PEFT	FFT	PEFT	FFT	PEFT	FFT	PEFT
CE	54.6	71.9	70.3	80.7	24.7	39.8	26.0	31.9
Focal	52.7	71.2	69.4	81.4	24.3	39.0	25.9	30.9
LDAM	53.6	73.6	64.4	82.8	24.7	41.1	25.0	30.9
CB	54.7	72.5	69.4	80.3	25.1	40.2	26.0	32.0
G-RW	50.9	71.8	66.9	81.8	22.0	44.5	23.4	34.2
BS	58.0	**80.1**	**75.8**	85.1	31.3	48.4	30.3	38.3
LA	**62.7**	79.8	73.1	**86.3**	**32.0**	48.0	**31.9**	**39.7**
LADE	18.2	79.9	72.8	86.0	16.8	**49.2**	27.3	0.3

In most cases, we find that Focal loss, Class-Balanced loss and Generalized Re-Weight loss achieve only moderate gains when applied to foundation models in both FFT and PEFT settings, and even impair the performance in some cases. LDAM loss shows a slight improvement only in the PEFT setting, with no improvement observed in the FFT setting. LADE loss is complex and highly sensitive to hyperparameter selection due to its two hyperparameters. We use the same parameters for

LADE across all experimental settings; however, in some cases, it provides a significant improvement, while in others, it leads to a notable performance drop and even causes training collapse. Figure 3 shows the training loss of the LADE under certain training settings, which fails to converge to lower values and even crashes during training, indicating the potential risk caused by improper hyperparameters. We believe the LADE loss function introduces numerous additional assumptions based on logit adjustment, making it overly complex. Therefore, it may only be suitable for specific models, such as CNN models, rather than ViT models.

In contrast, Balanced Softmax and Logit-Adjusted loss consistently proved to be effective methods for both FFT and PEFT in foundation models and can significantly improve model performance. Specifically, they sacrifice a little performance of the head class in exchange for significant improvements in the performance of the middle and tail classes. Based on the experimental results, we recommend using Balanced Softmax loss and Logit-Adjusted loss when fine-tuning foundation models with long-tailed datasets. If time spent on hyperparameter tuning is non-trivial, then the nonparametric BS loss is a more reliable choice.

3.5 Balanced Classifier

In general visual tasks, a common practice in deep learning is to employ linear classifiers $p = \phi(w \cdot x + b)$ for classification, where ϕ is the softmax function, the bias term b can be discarded. However, the long-tailed distribution data lead to larger classifier weight norms for head classes than tail classes (Yin et al., 2019). We investigate diverse classifier types to tackle this challenge.

Classifier Methods We introduce two representative classifiers, *i.e.*, Cosine classifier and τ-normalized classifier.

- Cosine classifier (Wu et al., 2021) uses a scale-invariant metric $p = \phi((\frac{w \cdot x}{||w|| \cdot ||x||})/t + b)$, in which both the classifier weights and the sample features are normalized. t is the temperature parameter. This strategy can be motivated by removing the negative impact of imbalanced weight norms (Kang et al., 2020; Wei et al., 2021).
- τ-normalized classifier (Kang et al., 2020) adjust the classifier weight norms to solve the imbalance by τ-normalized procedure, typically used to enhance the performance and stability of models in high-dimensional data. Formally, $\tilde{w} = \frac{w}{||w||_2^\tau}$, where τ is temperature factor for normalization.

Experimental Result In our experiments, we follow the setting of Shi et al. (2024) and Kang et al. (2020) and set the t to $\frac{1}{30}$ in Cosine Classifier and τ to $0.5, 1, 2$ in τ-normalized classifier. Table 6 shows the accuracy of different classifier methods on CIFAR100-LT and Places-LT datasets. For more detailed results, please refer to Appendix section D.4.

In our experiments, we observed comparable training costs across different classifiers. According to the experiment results, we can observe that in most cases, the Cosine classifier is a better choice because it has empirical robustness to imbalances and stronger generalization ability. Note that these classifiers are exclusive to each other and can't be used simultaneously. We recommend using the Cosine Classifier to train foundation models.

Table 6: Accuracy of applying different classifiers.

Datasets	CIFAR100-LT				Places-LT			
Backbone	CLIP		ViT		CLIP		ViT	
	FFT	PEFT	FFT	PEFT	FFT	PEFT	FFT	PEFT
Linear	54.6	71.9	**70.3**	80.7	**24.9**	39.8	26.0	31.9
Cosine	**56.4**	**72.2**	69.6	**83.9**	**24.9**	**40.6**	**27.1**	**38.1**
τ-norm ($\tau = 0.5$)	55.6	71.7	69.3	80.8	24.7	40.3	25.8	32.1
τ-norm ($\tau = 1$)	55.6	71.9	68.9	80.9	24.6	40.0	25.4	32.3
τ-norm ($\tau = 2$)	54.8	71.8	68.8	81.2	23.5	37.6	24.8	32.1

3.6 Other Tricks

In addition to the aforementioned methods, we also explore two more tricks: mixup (Zhang et al., 2018) and label smoothing (Szegedy et al., 2016), which are widely used in various types of deep models and long-tail learning algorithms (Zhong et al., 2021).

Table 7: Accuracy of applying mixup.

Datasets	CIFAR100-LT				Places-LT			
Backbone	CLIP		ViT		CLIP		ViT	
	FFT	PEFT	FFT	PEFT	FFT	PEFT	FFT	PEFT
Baseline	51.5	**80.1**	75.8	85.1	31.3	48.8	30.3	38.3
Mixup	**68.7**	79.7	**81.6**	**86.7**	**35.8**	**49.8**	**33.3**	**45.0**

Table 8: Accuracy of applying label smoothing.

Datasets	CIFAR100-LT				Places-LT			
Backbone	CLIP		ViT		CLIP		ViT	
	FFT	PEFT	FFT	PEFT	FFT	PEFT	FFT	PEFT
CE	54.6	**71.9**	70.3	80.7	24.7	**39.8**	26.0	31.9
CE (w/ LS)	**56.2**	71.7	**71.3**	**82.7**	**25.0**	39.7	**26.9**	**34.1**
BS	58.0	80.1	75.8	85.1	**31.3**	48.8	30.3	38.3
BS (w/ LS)	**59.8**	**80.6**	**78.2**	**88.1**	28.6	**49.4**	**32.4**	**41.8**

For the mixup trick, we follow the setting of Zhang et al. (2018). Specifically, we randomly select two data points (x_i, y_i), (x_j, y_j) from the original dataset and combine them through linear weighting. Formally,

$$\widehat{x} = \theta x_i + (1-\theta)x_j \tag{1}$$

$$\widehat{y} = \theta y_i + (1-\theta)y_j \tag{2}$$

where θ is randomly sampled from a Beta distribution $Beta(\zeta, \zeta)$. The mixup hyper-parameter ζ controls the strength of interpolation between feature-target pairs.

Label smoothing (Szegedy et al., 2016) transforms the training label from hard (one-hot) label to soft label, where the true label is considered to have a probability of $1-\epsilon$, and the remaining ϵ is shared across all classes. After using label smoothing, the modified probability distribution is formulated as follows:

$$P_i = \begin{cases} 1, & \text{if } y = i \\ 0, & \text{if } y \neq i \end{cases} \Rightarrow P_i = \begin{cases} 1-\epsilon, & \text{if } y = i \\ \frac{\epsilon}{K-1}, & \text{if } y \neq i \end{cases} \tag{3}$$

where i is the i-th class, K is the total number of classes and the hyperparameter ϵ determine the smooth level.

Experimental Result Table 7 and Table 8 show the test accuracy of using these two tricks. For more detailed results, please refer to Appendix section D.7.

For mixup, we set hyper-parameter ζ to 1. It can be observed that input mixup effectively provides better results compared to the baseline in both FFT and PEFT settings. Mixup can be seen as a form of data augmentation that combines multiple samples linearly, rather than applying transformations to a single sample. This linear behavior helps reduce the oscillations when the model predicts the out-of-distribution samples (Zhang et al., 2018). However, when combined with other long-tail learning methods, mixup may also not always gain benefits like those mentioned above in subsection Data Augmentation.

For label smoothing, we set the ϵ to 0.1 by the setting of Szegedy et al. (2016) and apply it to CE loss and BS loss. We find that label smoothing can effectively improve the final performance of CE loss and BS loss. More specifically, label smoothing enhances the performance of tail classes, as shown in tables 40, 41, 42 in the Appendix. Our results suggest the noise introduced by label smoothing effectively reduces the model's tendency to overly favor head-class samples, allowing for greater focus on tail-class samples.

4 The Ultimate Framework

Framework construction In the previous section, we review several classical methods. In this section, we analyze these methods from a more unified perspective. Specifically, we compare the different combinations of these methods to identify the best framework. It is worth noting that since re-sampling methods and class-sensitive losses both aim to re-balance the data distribution, their

Table 9: Results of the ablation experiments. “Avg.” represents the average of all experimental results listed front in the line. Δ represents the performance change against the previous line. The abbreviations are defined as follows: “Cos” = Cosine Classifier, “Sqrt” = Square-Root Sampling, “BS” = Balanced-Softmax, “LS” = Label Smoothing, “Aug” = Auto Augmentation.

Datasets						ImageNet-LT				iNaturalist 2018				**Avg.**	Δ
Backbone						CLIP		ViT		CLIP		ViT			
Cos	Sqrt	BS	LS	Aug	Mixup	FFT	PEFT	FFT	PEFT	FFT	PEFT	FFT	PEFT		
						48.7	70.5	50.8	78.2	58.4	69.5	57.8	73.6	63.4	-
✓						48.7	70.4	53.2	80.3	63.3	75.3	61.5	75.6	66.0	+2.6
✓	✓					60.1	74.7	71.5	82.6	68.4	76.8	72.3	79.0	73.2	+7.2
✓	✓	✓				63.2	77.0	73.4	83.6	70.9	79.3	75.0	81.1	75.4	+2.2
✓	✓	✓	✓			64.1	77.2	75.2	84.1	71.5	79.0	74.6	81.1	**75.9**	+0.5
✓	✓	✓	✓	✓		64.5	76.6	75.5	84.1	69.6	78.3	74.9	81.1	75.6	–0.3
✓	✓	✓	✓		✓	65.7	75.5	76.4	84.1	69.4	76.9	73.3	79.9	75.2	–0.4
✓	✓	✓	✓	✓	✓	63.9	74.9	77.0	84.2	48.7	74.6	72.3	79.4	71.9	–3.3

simultaneous application will over-emphasize tail classes and harm generalization. To balance these effects, we adopt Square-root sampling (a moderate re-sampling approach) and apply Balanced Softmax loss to the rectified distribution.

For our final framework, we integrate AutoAugment, Cosine classifier, Square-root sampling, Balanced Softmax loss, mixup, and label smoothing – all selected based on their excellent performance in previous experiments. We conduct ablation experiments on these methods under multiple settings, including different backbones such as CLIP and IN21K pre-trained ViT, and different fine-tuning methods such as full fine-tuning (FFT) and parameter-efficient fine-tuning (PEFT). The results are shown in Table 9. Due to the page limit, we report more detailed results for all datasets in Appendix section D.8.

From the results, we can conclude that 1) The combination methods of **Cosine Classifier**, **Square-root sampling**, **BS loss**, and **label smoothing** can **consistently** enhance the model performance on foundation models when using long-tailed data. As they achieve the best average performance across all scenarios, we consider the combination of these four methods as the optimal framework. 2) AutoAugment and mixup, as different forms of data augmentation, have **inconsistent** effects on performance across different datasets and models. There is no consistent conclusion on whether they improve or decrease performance based on our experiments, so we exclude them from the optimal framework.

Table 10: The results of applying our framework compared to other methods across four datasets: Places-LT, ImageNet-LT, CIFAR100-LT, iNaturalist 2018. † denotes VL-LTR uses extra data for fine-tuning. “-” means the paper has not reported the corresponding result. We also compare our framework with LIFT Shi et al. (2024) in Appendix D.9.

	Places-LT	IN-LT	CIFAR-LT	iNat.
MiSLAS (Zhong et al., 2021)	40.4	52.7	47.0	71.6
PaCo (Cui et al., 2021)	41.2	57.0	52.0	71.8
LiVT (Xu et al., 2023b)	40.8	60.9	58.2	76.1
BALLAD (Ma et al., 2021)	49.5	75.7	77.8	-
Decoder (Wang et al., 2024b)	46.8	73.2	-	59.2
LPT (Dong et al., 2023)	50.1	-	-	76.1
VL-LTR† (Tian et al., 2022)	50.1	**77.2**	-	76.8
Ours	**51.2**	**77.2**	**80.5**	**79.0**

Improvements over baselines We apply our ultimate framework to four datasets on the pre-trained CLIP-ViT-B/16 backbone and obtain quite competitive results under PEFT settings. The test accuracy is reported in Table 10. Overall, our framework achieves superior performance on these challenging datasets, surpassing Decoder, LPT, VL-LTR, and various training-from-scratch approaches. And VL-LTR relies on extensive auxiliary data to facilitate fine-tuning, the advantage of our framework is more significant compared with methods that do not use auxiliary data. In addition, due to the Square-root sampling method included in our framework, the training cost of our framework is significantly reduced compared to other methods.

To provide a deeper mechanistic analysis. We examine the classifier weight norms, which led to some interesting findings. Specifically, we extract the classifier weight norms from models trained under the PEFT setting of CLIP-ViT/B-16 using four different datasets. Figure 4 displays the classifier weight norms for Cifar100-IR100 and Places-LT. The classes on the horizontal axis are arranged in descending order of their number of training samples.

Figure 4: Classifier weight norms for CIFAR100-IR100 and Places-LT.

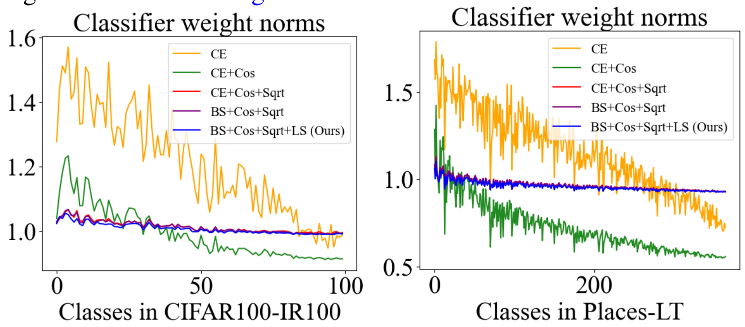

Due to the pronounced overlap between the curve of our method (blue line) and those of other approaches, visual inspection alone is insufficient to draw a definitive conclusion regarding its superior balance. To facilitate a quantitative comparison, we employ the standard deviation of the classifier weight norms as a metric for balance. The subsequent results are shown in Table 11 .

The results validate the superiority of our proposed method, which attains the most balanced norms — as evidenced by the lowest standard deviation in the comparison.

Table 11: Standard Deviation of classifier weight norms from models trained on different datasets. Each value in the table represents the actual standard deviation when multiplied by 10^{-2}.

Standard Deviation	Places-LT	IN-LT	CIFAR-LT	iNat.
CE	16.3	23.8	13.6	10.6
CE+Cos	7.9	15.2	7.8	5.7
CE+Cos+Sqrt	1.8	3.0	1.3	3.9
BS+Cos+Sqrt	1.8	3.0	1.3	3.9
BS+Cos+Sqrt+LS	**1.5**	**2.6**	**1.1**	**3.6**

Discussions We have taken into account the potential data leakage issue, such as between ImageNet and IN21K-ViT. In response to this, in Table 10, we only present results on CLIP-ViT-B/16. For detailed results across more experimental settings, we report in the Appendix. Looking ahead, we intend to explore the generalizability of our framework by extending it to more models, such as DINO (Oquab et al., 2023), which could further validate its transferability across different foundation models. Preliminary investigations in Appendix D.10 have already shown encouraging alignment with our current findings, suggesting broader applicability.

5 Conclusion

In this paper, we systematically revisit the representative long-tail learning methods and provide a scientific empirical guideline for their accurate use in fine-tuning foundation models. Furthermore, we select the optimal methods to construct a unified framework and analyze the contribution of each component through extensive ablation studies. Our proposed framework achieves competitive performance on multiple long-tailed datasets. We hope that our work serves as a convenient guideline for related applications and can inspire further research in the field of long-tail learning.

REFERENCES

Mateusz Buda, Atsuto Maki, and Maciej A Mazurowski. A systematic study of the class imbalance problem in convolutional neural networks. *Neural Networks*, 106:249–259, 2018.

Kaidi Cao, Colin Wei, Adrien Gaidon, Nikos Arechiga, and Tengyu Ma. Learning imbalanced datasets with label-distribution-aware margin loss. In *Advances in Neural Information Processing Systems*, volume 32, pp. 1565–1576, 2019.

Nitesh V Chawla, Kevin W Bowyer, Lawrence O Hall, and W Philip Kegelmeyer. Smote: synthetic minority over-sampling technique. *Journal of artificial intelligence research*, 16:321–357, 2002.

Shoufa Chen, Chongjian Ge, Zhan Tong, Jiangliu Wang, Yibing Song, Jue Wang, and Ping Luo. AdaptFormer: Adapting vision transformers for scalable visual recognition. *Advances in Neural Information Processing Systems*, 35:16664–16678, 2022.

Ekin D Cubuk, Barret Zoph, Dandelion Mane, Vijay Vasudevan, and Quoc V Le. Autoaugment: Learning augmentation strategies from data. In *Proceedings of the IEEE/CVF Conference on Computer Vision and Pattern Recognition*, pp. 113–123, 2019.

Ekin D Cubuk, Barret Zoph, Jonathon Shlens, and Quoc V Le. Randaugment: Practical automated data augmentation with a reduced search space. In *Proceedings of the IEEE/CVF Conference on Computer Vision and Pattern Recognition Workshops*, pp. 702–703, 2020.

Jiequan Cui, Zhisheng Zhong, Shu Liu, Bei Yu, and Jiaya Jia. Parametric contrastive learning. In *Proceedings of the IEEE/CVF International Conference on Computer Vision*, pp. 715–724, 2021.

Yin Cui, Yang Song, Chen Sun, Andrew Howard, and Serge Belongie. Large scale fine-grained categorization and domain-specific transfer learning. In *Proceedings of the IEEE conference on Computer Vision and Pattern Recognition*, pp. 4109–4118, 2018.

Yin Cui, Menglin Jia, Tsung-Yi Lin, Yang Song, and Serge Belongie. Class-balanced loss based on effective number of samples. In *Proceedings of the IEEE/CVF Conference on Computer Vision and Pattern Recognition*, pp. 9268–9277, 2019.

Mostafa Dehghani, Josip Djolonga, Basil Mustafa, Piotr Padlewski, Jonathan Heek, Justin Gilmer, Andreas Peter Steiner, Mathilde Caron, Robert Geirhos, Ibrahim Alabdulmohsin, et al. Scaling vision transformers to 22 billion parameters. In *International Conference on Machine Learning*, pp. 7480–7512. PMLR, 2023.

Jia Deng, Wei Dong, Richard Socher, Li-Jia Li, Kai Li, and Li Fei-Fei. Imagenet: A large-scale hierarchical image database. In *IEEE Conference on Computer Vision and Pattern Recognition*, pp. 248–255. Ieee, 2009.

Bowen Dong, Pan Zhou, Shuicheng Yan, and Wangmeng Zuo. LPT: Long-tailed prompt tuning for image classification. In *The Eleventh International Conference on Learning Representations*, 2023. URL `https://openreview.net/forum?id=8pOVAeo8ie`.

Alexey Dosovitskiy, Lucas Beyer, Alexander Kolesnikov, Dirk Weissenborn, Xiaohua Zhai, Thomas Unterthiner, Mostafa Dehghani, Matthias Minderer, Georg Heigold, Sylvain Gelly, Jakob Uszkoreit, and Neil Houlsby. An image is worth 16x16 words: Transformers for image recognition at scale. In *International Conference on Learning Representations*, 2021.

Peng Gao, Shijie Geng, Renrui Zhang, Teli Ma, Rongyao Fang, Yongfeng Zhang, Hongsheng Li, and Yu Qiao. Clip-adapter: Better vision-language models with feature adapters. *International Journal of Computer Vision*, 132(2):581–595, 2024.

Kaiming He, Xiangyu Zhang, Shaoqing Ren, and Jian Sun. Deep residual learning for image recognition. In *Proceedings of the IEEE conference on Computer Vision and Pattern Recognition*, pp. 770–778, 2016.

Youngkyu Hong, Seungju Han, Kwanghee Choi, Seokjun Seo, Beomsu Kim, and Buru Chang. Disentangling label distribution for long-tailed visual recognition. In *Proceedings of the IEEE/CVF Conference on Computer Vision and Pattern Recognition*, pp. 6626–6636, 2021.

Menglin Jia, Luming Tang, Bor-Chun Chen, Claire Cardie, Serge Belongie, Bharath Hariharan, and Ser-Nam Lim. Visual prompt tuning. In *Proceedings of the 17th European Conference on Computer Vision*, pp. 709–727, 2022.

Bingyi Kang, Saining Xie, Marcus Rohrbach, Zhicheng Yan, Albert Gordo, Jiashi Feng, and Yannis Kalantidis. Decoupling representation and classifier for long-tailed recognition. In *International Conference on Learning Representations*, 2020.

Bingyi Kang, Yu Li, Sa Xie, Zehuan Yuan, and Jiashi Feng. Exploring balanced feature spaces for representation learning. In *International Conference on Learning Representations*, 2021.

Salman Khan, Munawar Hayat, Syed Waqas Zamir, Jianbing Shen, and Ling Shao. Striking the right balance with uncertainty. In *Proceedings of the IEEE/CVF Conference on Computer Vision and Pattern Recognition*, pp. 103–112, 2019.

A Krizhevsky. Learning multiple layers of features from tiny images. *Master's thesis, University of Tront*, 2009.

Alex Krizhevsky, Ilya Sutskever, and Geoffrey E Hinton. Imagenet classification with deep convolutional neural networks. *Advances in Neural Information Processing Systems*, 25, 2012.

Ananya Kumar, Aditi Raghunathan, Robbie Matthew Jones, Tengyu Ma, and Percy Liang. Fine-tuning can distort pretrained features and underperform out-of-distribution. In *International Conference on Learning Representations*, 2022.

Tsung-Yi Lin, Priya Goyal, Ross Girshick, Kaiming He, and Piotr Dollár. Focal loss for dense object detection. In *Proceedings of the IEEE International Conference on Computer Vision*, pp. 2980–2988, 2017.

Bo Liu, Haoxiang Li, Hao Kang, Gang Hua, and Nuno Vasconcelos. Gistnet: a geometric structure transfer network for long-tailed recognition. In *Proceedings of the IEEE/CVF International Conference on Computer Vision*, pp. 8209–8218, 2021a.

Xu-Ying Liu, Jianxin Wu, and Zhi-Hua Zhou. Exploratory undersampling for class-imbalance learning. *IEEE Transactions on Systems, Man, and Cybernetics, Part B (Cybernetics)*, 39(2):539–550, 2008.

Ze Liu, Yutong Lin, Yue Cao, Han Hu, Yixuan Wei, Zheng Zhang, Stephen Lin, and Baining Guo. Swin transformer: Hierarchical vision transformer using shifted windows. In *Proceedings of the IEEE/CVF International Conference on Computer Vision*, pp. 10012–10022, 2021b.

Ziwei Liu, Zhongqi Miao, Xiaohang Zhan, Jiayun Wang, Boqing Gong, and Stella X Yu. Large-scale long-tailed recognition in an open world. In *Proceedings of the IEEE/CVF Conference on Computer Vision and Pattern Recognition*, pp. 2537–2546, 2019.

Alexander Long, Wei Yin, Thalaiyasingam Ajanthan, Vu Nguyen, Pulak Purkait, Ravi Garg, Alan Blair, Chunhua Shen, and Anton van den Hengel. Retrieval augmented classification for long-tail visual recognition. In *Proceedings of the IEEE/CVF Conference on Computer Vision and Pattern Recognition*, pp. 6959–6969, June 2022.

Teli Ma, Shijie Geng, Mengmeng Wang, Jing Shao, Jiasen Lu, Hongsheng Li, Peng Gao, and Yu Qiao. A simple long-tailed recognition baseline via vision-language model. *arXiv preprint arXiv:2111.14745*, 2021.

Aditya Krishna Menon, Sadeep Jayasumana, Ankit Singh Rawat, Himanshu Jain, Andreas Veit, and Sanjiv Kumar. Long-tail learning via logit adjustment. In *International Conference on Learning Representations*, 2021.

Ajinkya More. Survey of resampling techniques for improving classification performance in unbalanced datasets. *arXiv preprint arXiv:1608.06048*, 2016.

Maxime Oquab, Timothée Darcet, Théo Moutakanni, Huy Vo, Marc Szafraniec, Vasil Khalidov, Pierre Fernandez, Daniel Haziza, Francisco Massa, Alaaeldin El-Nouby, et al. Dinov2: Learning robust visual features without supervision. *arXiv preprint arXiv:2304.07193*, 2023.

Alec Radford, Jong Wook Kim, Chris Hallacy, Aditya Ramesh, Gabriel Goh, Sandhini Agarwal, Girish Sastry, Amanda Askell, Pamela Mishkin, Jack Clark, et al. Learning transferable visual models from natural language supervision. In *International Conference on Machine Learning*, pp. 8748–8763. PMLR, 2021.

Harsh Rangwani, Sumukh K Aithal, Mayank Mishra, et al. Escaping saddle points for effective generalization on class-imbalanced data. *Advances in Neural Information Processing Systems*, 35:22791–22805, 2022.

Harsh Rangwani, Pradipto Mondal, Mayank Mishra, Ashish Ramayee Asokan, and R Venkatesh Babu. DeiT-LT: Distillation strikes back for vision transformer training on long-tailed datasets. In *Proceedings of the IEEE/CVF Conference on Computer Vision and Pattern Recognition*, pp. 23396–23406, 2024.

Jiawei Ren, Cunjun Yu, Xiao Ma, Haiyu Zhao, Shuai Yi, et al. Balanced meta-softmax for long-tailed visual recognition. *Advances in Neural Information Processing Systems*, 33:4175–4186, 2020.

Saurabh Sharma, Ning Yu, Mario Fritz, and Bernt Schiele. Long-tailed recognition using class-balanced experts. In *Pattern Recognition: 42nd DAGM German Conference, DAGM GCPR 2020, Tübingen, Germany, September 28–October 1, 2020, Proceedings 42*, pp. 86–100. Springer, 2021.

Jiang-Xin Shi, Tong Wei, Yuke Xiang, and Yu-Feng Li. How re-sampling helps for long-tail learning? In *Advances in Neural Information Processing Systems*, volume 36, pp. 75669–75687, 2023.

Jiang-Xin Shi, Tong Wei, Zhi Zhou, Jie-Jing Shao, Xin-Yan Han, and Yu-Feng Li. Long-tail learning with foundation model: Heavy fine-tuning hurts. In *Forty-first International Conference on Machine Learning*, 2024.

Connor Shorten and Taghi M Khoshgoftaar. A survey on image data augmentation for deep learning. *Journal of Big Data*, 6(1):1–48, 2019.

Christian Szegedy, Vincent Vanhoucke, Sergey Ioffe, Jon Shlens, and Zbigniew Wojna. Rethinking the inception architecture for computer vision. In *Proceedings of the IEEE conference on Computer Vision and Pattern Recognition*, pp. 2818–2826, 2016.

Jingru Tan, Changbao Wang, Buyu Li, Quanquan Li, Wanli Ouyang, Changqing Yin, and Junjie Yan. Equalization loss for long-tailed object recognition. In *Proceedings of the IEEE/CVF Conference on Computer Vision and Pattern Recognition*, pp. 11662–11671, 2020.

Changyao Tian, Wenhai Wang, Xizhou Zhu, Jifeng Dai, and Yu Qiao. VL-LTR: Learning class-wise visual-linguistic representation for long-tailed visual recognition. In *Proceedings of the 17th European Conference on Computer Vision*, pp. 73–91. Springer, 2022.

Hugo Touvron, Matthieu Cord, Matthijs Douze, Francisco Massa, Alexandre Sablayrolles, and Hervé Jégou. Training data-efficient image transformers & distillation through attention. In *International Conference on Machine Learning*, pp. 10347–10357. PMLR, 2021.

Grant Van Horn, Oisin Mac Aodha, Yang Song, Yin Cui, Chen Sun, Alex Shepard, Hartwig Adam, Pietro Perona, and Serge Belongie. The inaturalist species classification and detection dataset. In *Proceedings of the IEEE conference on Computer Vision and Pattern Recognition*, pp. 8769–8778, 2018.

Ashish Vaswani, Noam Shazeer, Niki Parmar, Jakob Uszkoreit, Llion Jones, Aidan N Gomez, Łukasz Kaiser, and Illia Polosukhin. Attention is all you need. In *Advances in Neural Information Processing Systems*, volume 30, pp. 5998–6008, 2017.

Athanasios Voulodimos, Nikolaos Doulamis, Anastasios Doulamis, and Eftychios Protopapadakis. Deep learning for computer vision: A brief review. *Computational Intelligence and Neuroscience*, 2018(1):7068349, 2018.

Mengmeng Wang, Jiazheng Xing, and Yong Liu. Actionclip: A new paradigm for video action recognition. *arXiv preprint arXiv:2109.08472*, 2021a.

Pengkun Wang, Zhe Zhao, HaiBin Wen, Fanfu Wang, Binwu Wang, Qingfu Zhang, and Yang Wang. LLM-autoDA: Large language model-driven automatic data augmentation for long-tailed problems. In *The Thirty-eighth Annual Conference on Neural Information Processing Systems*, 2024a.

Xudong Wang, Long Lian, Zhongqi Miao, Ziwei Liu, and Stella Yu. Long-tailed recognition by routing diverse distribution-aware experts. In *International Conference on Learning Representations*, 2021b.

Yidong Wang, Zhuohao Yu, Jindong Wang, Qiang Heng, Hao Chen, Wei Ye, Rui Xie, Xing Xie, and Shikun Zhang. Exploring vision-language models for imbalanced learning. *International Journal of Computer Vision*, 132(1):224–237, 2024b.

Tong Wei, Wei-Wei Tu, Yu-Feng Li, and Guo-Ping Yang. Towards robust prediction on tail labels. In *Proceedings of the 27th ACM SIGKDD Conference on Knowledge Discovery & Data Mining*, pp. 1812–1820, 2021.

Tong Wu, Qingqiu Huang, Ziwei Liu, Yu Wang, and Dahua Lin. Distribution-balanced loss for multi-label classification in long-tailed datasets. In *Computer Vision–ECCV 2020: 16th European Conference, Glasgow, UK, August 23–28, 2020, Proceedings, Part IV 16*, pp. 162–178. Springer, 2020.

Tong Wu, Ziwei Liu, Qingqiu Huang, Yu Wang, and Dahua Lin. Adversarial robustness under long-tailed distribution. In *Proceedings of the IEEE/CVF Conference on Computer Vision and Pattern Recognition*, pp. 8659–8668, 2021.

Liuyu Xiang, Guiguang Ding, and Jungong Han. Learning from multiple experts: Self-paced knowledge distillation for long-tailed classification. In *Computer Vision–ECCV 2020: 16th European Conference, Glasgow, UK, August 23–28, 2020, Proceedings, Part V 16*, pp. 247–263. Springer, 2020.

Mengde Xu, Zheng Zhang, Fangyun Wei, Han Hu, and Xiang Bai. Side adapter network for open-vocabulary semantic segmentation. In *Proceedings of the IEEE/CVF Conference on Computer Vision and Pattern Recognition*, pp. 2945–2954, June 2023a.

Zhengzhuo Xu, Ruikang Liu, Shuo Yang, Zenghao Chai, and Chun Yuan. Learning imbalanced data with vision transformers. In *Proceedings of the IEEE/CVF Conference on Computer Vision and Pattern Recognition*, pp. 15793–15803, June 2023b.

Bin Yan, Yi Jiang, Jiannan Wu, Dong Wang, Ping Luo, Zehuan Yuan, and Huchuan Lu. Universal instance perception as object discovery and retrieval. In *Proceedings of the IEEE/CVF Conference on Computer Vision and Pattern Recognition*, pp. 15325–15336, June 2023.

Lu Yang, He Jiang, Qing Song, and Jun Guo. A survey on long-tailed visual recognition. *International Journal of Computer Vision*, 130(7):1837–1872, 2022.

Xi Yin, Xiang Yu, Kihyuk Sohn, Xiaoming Liu, and Manmohan Chandraker. Feature transfer learning for face recognition with under-represented data. In *Proceedings of the IEEE/CVF Conference on Computer Vision and Pattern Recognition*, pp. 5704–5713, 2019.

Kun Yuan, Shaopeng Guo, Ziwei Liu, Aojun Zhou, Fengwei Yu, and Wei Wu. Incorporating convolution designs into visual transformers. In *Proceedings of the IEEE/CVF International Conference on Computer Vision*, pp. 579–588, 2021a.

Li Yuan, Yunpeng Chen, Tao Wang, Weihao Yu, Yujun Shi, Zi-Hang Jiang, Francis E.H. Tay, Jiashi Feng, and Shuicheng Yan. Tokens-to-token vit: Training vision transformers from scratch on imagenet. In *Proceedings of the IEEE/CVF International Conference on Computer Vision (ICCV)*, pp. 558–567, October 2021b.

Elad Ben Zaken, Yoav Goldberg, and Shauli Ravfogel. Bitfit: Simple parameter-efficient fine-tuning for transformer-based masked language-models. In *Proceedings of the 60th Annual Meeting of the Association for Computational Linguistics (Volume 2: Short Papers)*, pp. 1–9, 2022.

Hongyi Zhang, Moustapha Cisse, Yann N. Dauphin, and David Lopez-Paz. mixup: Beyond empirical risk minimization. In *International Conference on Learning Representations*, 2018.

Songyang Zhang, Zeming Li, Shipeng Yan, Xuming He, and Jian Sun. Distribution alignment: A unified framework for long-tail visual recognition. In *Proceedings of the IEEE/CVF Conference on Computer Vision and Pattern Recognition*, pp. 2361–2370, 2021a.

Yifan Zhang, Bingyi Kang, Bryan Hooi, Shuicheng Yan, and Jiashi Feng. Deep long-tailed learning: A survey. *IEEE Transactions on Pattern Analysis and Machine Intelligence*, 45(9):10795–10816, 2023.

Yongshun Zhang, Xiu-Shen Wei, Boyan Zhou, and Jianxin Wu. Bag of tricks for long-tailed visual recognition with deep convolutional neural networks. In *AAAI*, pp. 3447–3455, 2021b.

Zhong-Qiu Zhao, Peng Zheng, Shou-tao Xu, and Xindong Wu. Object detection with deep learning: A review. *IEEE transactions on Neural Networks and Learning Systems*, 30(11):3212–3232, 2019.

Zhisheng Zhong, Jiequan Cui, Shu Liu, and Jiaya Jia. Improving calibration for long-tailed recognition. In *Proceedings of the IEEE/CVF Conference on Computer Vision and Pattern Recognition*, pp. 16489–16498, June 2021.

Bolei Zhou, Agata Lapedriza, Aditya Khosla, Aude Oliva, and Antonio Torralba. Places: A 10 million image database for scene recognition. *IEEE Transactions on Pattern Analysis and Machine Intelligence*, 40(6):1452–1464, 2017.

Boyan Zhou, Quan Cui, Xiu-Shen Wei, and Zhao-Min Chen. Bbn: Bilateral-branch network with cumulative learning for long-tailed visual recognition. In *Proceedings of the IEEE/CVF Conference on Computer Vision and Pattern Recognition*, pp. 9719–9728, 2020.

Kaiyang Zhou, Jingkang Yang, Chen Change Loy, and Ziwei Liu. Learning to prompt for vision-language models. *International Journal of Computer Vision*, 130(9):2337–2348, 2022.

Jianggang Zhu, Zheng Wang, Jingjing Chen, Yi-Ping Phoebe Chen, and Yu-Gang Jiang. Balanced contrastive learning for long-tailed visual recognition. In *Proceedings of the IEEE/CVF Conference on Computer Vision and Pattern Recognition*, pp. 6908–6917, 2022.

Zhengxia Zou, Keyan Chen, Zhenwei Shi, Yuhong Guo, and Jieping Ye. Object detection in 20 years: A survey. *Proceedings of the IEEE*, 111(3):257–276, 2023.

A Experimental Settings

A.1 Datasets

CIFAR100-LT CIFAR100-LT is the long-tailed version of CIFAR (Krizhevsky, 2009). The latter is a balanced dataset consisting of 100 classes, with each class containing 500 samples for training and 100 samples for test. We construct CIFAR100-LT following the approach in (Cao et al., 2019). Specifically, each class contains $n_i = 500 \cdot r^{(-\frac{i-1}{99})}$ samples in training, where i is class index. In this work, the imbalance factor is set to 100 considering its generality (Shi et al., 2024; Ma et al., 2021; Rangwani et al., 2022).

Places-LT The Places-LT (Sharma et al., 2021) features a long-tailed dataset consisting of 62,500 images across 365 classes from Places-2 (Zhou et al., 2017). The class frequencies follow a natural power law distribution, with the largest class containing 4,980 images and the smallest class containing only 5 images.

ImageNet-LT ImageNet-LT (Liu et al., 2019) is a long-tailed version of ImageNet ILSVRC 2012 (Deng et al., 2009), composed according to a Pareto distribution. This dataset consists of 1000 classes and a total of 1158K images, with the largest class containing up to 1,280 images and the smallest class containing as few as 5 images.

iNaturalist 2018 iNaturalist 2018 (Van Horn et al., 2018) is a natural dataset of fine-grained long-tailed categories, consisting of wildlife images across 8,142 species, with a total of 437,513 images. The number of images in each category ranges from a maximum of 1000 to a minimum of 2. It is a standard benchmark for evaluating algorithm performance on long-tailed distribution tasks.

A.2 Implementation Settings

In most of our experiments, we adopt pre-trained model CLIP (Radford et al., 2021) and Vision Transformer (Dosovitskiy et al., 2021) as the backbone and employ full fine-tuning (FFT) and parameter-efficient fine-tuning (PEFT) on these two models. Knowledge distillation is an exception where we use pre-trained DeiT (Touvron et al., 2021) as the student backbone. For the PEFT methods, we choose AdaptFormer (Chen et al., 2022) because of its optimal performance (Shi et al., 2024). Table 12 shows the performance of different PEFT methods under the ultimate framework. We use the SGD optimizer with a batch size of 128, weight decay of $5 \cdot 10^{-4}$, and momentum of 0.9. The number of training epochs for iNaturalist 2018 is 100, while for other datasets, it is 50. The learning rate is initialized to 0.1. The number of epochs and learning rate are carefully selected. We conduct comprehensive ablation studies on the epochs and learning rates across the CIFAR100-IR100, Places-LT, and ImageNet-LT datasets as shown in Table 13. We use mean accuracy and harmonic mean accuracy to measure the model's performance. In addition, we also follow the evaluation protocol introduced by (Liu et al., 2019), reporting accuracy for three categories: many-shot (>100 images), medium-shot (20-100 images), and few-shot (<20 images).

Table 12: Accuracy of using different PEFT methods.

Datasets	Places-LT		ImageNet-LT	
Backbone	CLIP	ViT	CLIP	ViT
LoRA	50.7	47.1	76.0	83.8
VPT-deep	50.5	47.5	76.2	**84.1**
Adapter	50.9	47.7	77.0	84.0
Bias-tuning	50.9	47.3	76.2	83.2
AdapterFormer	**51.2**	**47.9**	**77.2**	**84.1**

B Knowledge Distillation

In this subsection, we focus on the knowledge distillation technique and explore whether it can improve the performance of long-tailed datasets on foundation models. We follow the setup mentioned in Data Efficient Transformer (DeiT) Touvron et al. (2021) to create the student backbone for our

Table 13: Comparison of different numbers of epochs and learning rate.

		CIFAR100-IR100	Places-LT	ImageNet-LT
Epochs	10	78.7	50.7	75.7
	20	80.2	**51.3**	77.0
	50	**80.8**	51.2	**77.2**
	70	80.7	50.8	77.0
	90	80.4	50.4	76.8
LR	0.001	78.7	49.8	74.4
	0.005	**80.8**	**51.5**	76.9
	0.01	**80.8**	51.2	**77.2**
	0.05	77.9	48.9	75.7
	0.1	77.1	48.3	75.3

experiments. In addition to the CLS token, DeiT adds a DIST token in the ViT backbone that learns via distillation from the teacher. For both the classification head and the distillation head, training is conducted using cross-entropy loss, and the final loss function Rangwani et al. (2024) is

$$\mathcal{L} = aL_{CE}(f^{cls}(x), y) + (1 - a)L_{CE}(f^{dis}(x), y_t) \tag{4}$$

where $f^{cls}(x)$ and $f^{dis}(x)$ are outputs of the CLS and DIST tokens through their respective layers, y is the ground truth, and y_t is the teacher model's hard label for sample x.

Experimental Result We simply set the a to 0.5 to ensure the fair status of the ground truth and the teacher's prediction. Table 14 shows the accuracy of the knowledge distillation methods. For more detailed settings and results, please refer to Appendix section D.5.

Compared to PEFT, the performance enhancement under FFT is significantly more substantial. Experimental results demonstrate that knowledge distillation yields an improvement of approximately 3% in the FFT setting, whereas it contributes almost no gain in the PEFT setting.

We believe this is because knowledge distillation helps mitigate the biases towards the head classes in the student model during training. Since the FFT setting involves substantially more parameters to train compared to the PEFT setting, it is more susceptible to being biased toward head classes. This explains why the performance improvements are more pronounced in the FFT setting.

Table 14: Student results of applying knowledge distillation.

Datasets	CIFAR100-LT				Places-LT			
Student	DeiT-S		DeiT-Ti		DeiT-S		DeiT-Ti	
	FFT	PEFT	FFT	PEFT	FFT	PEFT	FFT	PEFT
Baseline	67.3	69.9	58.7	**60.8**	27.1	32.1	24.6	29.4
Distillation	**70.4**	**70.0**	**61.7**	60.6	**30.2**	**32.5**	**28.6**	**30.0**

C Ensemble Learning

Ensemble learning improves model performance by combining the predictions of multiple experts to address the long-tail problem. We conduct an experiment using a framework similar to BBN Zhou et al. (2020). Specifically, we use two branches: the "conventional learning branch", which employs the uniform sampler to learn the original data distribution, and the "re-balancing branch", which uses the reversed sampler to sample more tail-class samples for learning a balanced distribution. Both branches use the same backbone and share all the weights except for the last classifier. At last, a cumulative loss weight w is used to shift the learning "attention" smoothly from the head class to the tail class. Formally, the objective loss of the model is illustrated as

$$\mathcal{L} = wL_{CE}(f^c(x^c),y^c) + (1 - w)L_{CE}(f^r(x^r), y^r) \tag{5}$$

$$w = 1 - (\frac{t_c}{t_{max}})^2 \tag{6}$$

where the $f^c(x^c)$ and $f^r(x^r)$ respectively represent the predicted output of the conventional learning branch and re-balancing branch. y^c and y^r are the ground truth of x^c and x^r respectively. t_c and t_{max} respectively refer to the current epoch and total training epochs.

Experimental Result Ensemble-based methods address the class imbalance at the model level. Table 15 shows the accuracy of the ensemble method. For more detailed results, please refer to Appendix section D.6. Ensemble methods can generally improve performance by an average of over 3% in the PEFT setting. However, in the FFT setting, the model improvements are less favorable, with a maximum increase of 1%, and in some cases, even face a significant decrease.

Additionally, it is very important to note that ensemble learning inevitably increases the training cost. In this experiment, using two branches **doubles** the memory cost and computational time expenditure, because we need to create two individual data samplers and calculate the corresponding loss. In practice, though more experts may lead to better performance, the greater time and storage costs are non-negligible overheads. Therefore, we only recommend employing ensemble learning in the lightweight PEFT setting on foundation models. Using ensemble learning in the FFT setting is not cost-effective and does not guarantee performance improvements.

Table 15: Accuracy of applying ensemble learning.

Datasets	CIFAR100-LT				Places-LT			
Backbone	CLIP		ViT		CLIP		ViT	
	FFT	PEFT	FFT	PEFT	FFT	PEFT	FFT	PEFT
Baseline	54.6	71.9	**70.3**	80.7	**24.9**	39.8	26.0	31.9
Ensemble	**55.6**	**76.0**	68.6	**82.2**	18.9	**45.0**	**26.7**	**36.4**

D Additional Results

D.1 Re-sampling Detailed Results

For re-sampling methods, we report detailed results of applying RUS, RUSxN, ROS, EQ, Square-root sampling and no resampling (Baseline) methods. Tables 16, 17, 18 show the detailed results of applying re-sampling methods for CIFAR100-LT. Places-LT, ImageNet-LT respectively. Tables 19, 20, 21 show the detailed results of applying RUSxN for CIFAR100-LT, Places-LT and ImageNet-LT respectively. We can observe that applying RUS and Square-root sampling can significantly improve model performance.

D.2 Data Augmentation Detailed Results

For data augmentation methods, we report detailed results of applying ColorJitter, RandAugment, AutoAugment, and no augmentation (Baseline) methods. Tables 22, 23, 24 show the detailed results of applying data augmentation methods for CIFAR100-LT, Places-LT, ImageNet-LT respectively. We can observe that applying data augmentation methods can only slightly improve the model performance and don't play a decisive role.

D.3 Class-sensitive Loss Detailed Results

For Class-sensitive loss, we report detailed results of applying CE, Focal, Label-Distribution-Aware Margin, Class-Balanced, Generalized Re-Weight, Balanced Softmax, Logit Adjustment, LAbel distribution DisEntangling loss. The selection of hyperparameters for each loss follows the corresponding paper, except for G-RW. The original paper of G-RW proposed $\rho = 1.2$, which performs very poorly under FFT settings for each backbone. After our experimental attempts, we finally changed it to 0.5. The selected hyperparameters are shown as follows:

Focal loss: $\gamma = 2$; LDAM loss: $s = 25$; Class Balanced loss: $\beta = 0.9$; Generalized Re-weight loss: $\rho = 0.5$ for FFT setting, $\rho = 1.2$ for PEFT setting; Logit adjustment loss: $\mu = 1.5$; LADE loss: $\alpha = 0.01, \lambda = 0.1$.

In practice, we have tried different hyperparameters but only report the best. For example, we have tried: $\gamma = \{2, 3, 4\}$ for Focal loss; $\beta = \{0.9, 0.99, 0.999\}$ for Class-Balanced loss; $\tau = \{1, 1.5, 2\}$ for LA loss; $\rho = \{0.5, 1, 1.2, 1.5, 2\}$ for G-RW loss.

Tables 25, 26, 27 show the detailed results of applying class-sensitive losses for CIFAR100-LT, Places-LT, ImageNet-LT respectively. We can observe that applying Balanced Softmax loss and Logit Adjustment loss can greatly gain benefits.

D.4 Balanced Classifier Detailed Results

For the balanced classifier, we report detailed results of using the Cosine classifier, τ-normalized classifier, and Linear classifier methods. Tables 28, 29, 30 show the detailed results of applying different classifiers for CIFAR100-LT, Places-LT, ImageNet-LT respectively. We can observe that Cosine classifier can achieve an improvement in model performance.

D.5 Knowledge Distillation Detailed Results

We use a well-trained CLIP-ViT-B/16 as the teacher backbone for Places-LT and IN21K-ViT-B/16 as the teacher backbone for CIFAR100-LT and ImageNet-LT, while employing the pre-trained DeiT-S and DeiT-Ti backbone architecture as student models for all the datasets. Tables 31, 32, 33 show the detailed results of applying knowledge distillation on CIFAR100-LT, Places-LT, ImageNet-LT respectively. We can observe that knowledge distillation is only effective in the FFT setting.

D.6 Ensemble Learning Detailed Results

We build a framework similar to BBN and report details results of applying it on CIFAR100-LT, Places-LT and ImageNet-LT as shown in Tables 34, 35, 36 respectively. We can observe that applying ensemble learning is only cost-effective under the PEFT setting.

D.7 Tricks Detailed Results

For tricks, we report detailed results of applying mixup and label smoothing. Tables 37, 38, 39 show the detailed results of applying mixup for CIFAR100-LT, Places-LT, ImageNet-LT respectively. Tables 40, 41, 42 show the detailed results of applying label smoothing for CIFAR100-LT, Places-LT, ImageNet-LT respectively. We can observe that both tricks can improve model performance.

D.8 Ablation Experiments Detailed Results

To build the best framework for fine-tuning pre-trained models, we choose AutoAugment, Cosine classifier, Square-root resampling, Balanced Softmax loss, Mixup, and Label smoothing for the ablation experiments.

Tables 43, 44, 45, 46 show the detailed ablation results for CIFAR100-LT, Places-LT, ImageNet-LT, iNaturalist 2018 datasets respectively.

D.9 Comparison with LIFT

The performance of our model is comparable to that achieved by LIFT, as shown in the tables 47. Although we have more epochs, due to the sampling strategy of the data, the total training cost is significantly lower compared to LIFT, **with an average saved cost of 21%** (specific values vary depending on the dataset). Notably, it achieves a remarkable 34% reduction on the Places-LT, demonstrating the effectiveness of our method.

D.10 Transferability of our framework

To verify the transferability of our framework, we extend it to DINO and conduct corresponding experiments. The results are shown in Table 48. we are temporarily unable to report results for DINOv2 due to GPU memory limitations. Our framework can also be readily adapted to MAE and SigLIP, which are planned for a future version.

Table 16: Detailed results of applying resampling methods to the CIFAR100-LT dataset.

			Mean	Many	Med.	Few	Harmonic mean	Worst case
CLIP-ViT-B/16	FFT	Baseline	54.6	82.9	55.9	20.1	0.0	0.0
		Random Over-Sampling	44.8	77.7	42.5	9.1	0.0	0.0
		Random Under-Sampling	45.5	51.0	49.8	34.1	31.0	6.0
		Equal resampling	50.4	82.6	50.5	12.8	0.0	0.0
		Square-root resampling	56.8	80.3	60.0	25.8	0.1	0.0
	PEFT	Baseline	71.9	90.2	75.1	46.6	56.0	7.0
		Random Over-Sampling	68.3	89.0	73.1	38.5	36.9	2.0
		Random Under-Sampling	77.4	79.9	79.1	72.5	73.6	26.0
		Equal resampling	72.8	88.6	77.2	49.2	55.9	7.0
		Square-root resampling	76.4	87.1	78.2	61.8	69.8	18.0
IN21K-ViT-B/16	FFT	Baseline	70.3	89.6	71.9	45.8	48.0	3.0
		Random Over-Sampling	48.3	83.4	46.0	10.0	0.0	0.0
		Random Under-Sampling	69.3	74.6	71.6	60.3	58.5	5.0
		Equal resampling	62.0	90.0	64.6	26.2	0.0	0.0
		Square-root resampling	76.0	90.5	78.1	56.6	60.2	5.0
	PEFT	Baseline	80.7	93.5	80.9	65.4	41.2	1.0
		Random Over-Sampling	71.0	93.0	76.3	39.2	0.1	0.0
		Random Under-Sampling	87.0	90.5	87.3	82.6	81.9	15.0
		Equal resampling	77.3	93.1	80.3	55.3	37.3	1.0
		Square-root resampling	84.4	93.8	85.1	72.6	69.2	7.0

Table 17: Detailed results of applying resampling methods to the Places-LT dataset.

			Mean	Many	Med.	Few	Harmonic mean	Worst case
CLIP-ViT-B/16	FFT	Baseline	24.7	40.5	19.8	6.8	0.1	0.0
		Random Over-Sampling	12.6	25.7	7.2	0.7	0.0	0.0
		Random Under-Sampling	42.3	42.6	45.4	34.5	0.2	0.0
		Equal resampling	21.7	40.2	14.7	3.6	0.0	0.0
		Square-root resampling	37.1	51.0	34.8	16.6	18.8	1.0
	PEFT	Baseline	39.8	54.0	35.7	22.7	0.1	0.0
		Random Over-Sampling	38.3	51.0	35.5	20.9	0.4	0.0
		Random Under-Sampling	50.8	49.6	52.2	49.6	35.7	1.0
		Equal resampling	43.7	53.3	42.8	27.9	25.2	1.0
		Square-root resampling	47.5	55.6	45.7	36.6	32.4	2.0
IN21K-ViT-B/16	FFT	Baseline	26.0	41.4	20.9	9.5	0.1	0.0
		Random Over-Sampling	11.4	24.2	5.7	0.7	0.0	0.0
		Random Under-Sampling	41.2	47.6	43.3	24.6	23.4	1.0
		Equal resampling	22.0	40.4	14.9	4.2	0.0	0.0
		Square-root resampling	32.6	48.6	27.7	14.1	0.2	0.0
	PEFT	Baseline	32.1	45.9	28.4	15.2	0.2	0.0
		Random Over-Sampling	32.2	45.8	28.9	14.9	0.1	0.0
		Random Under-Sampling	45.3	46.7	47.6	37.5	32.2	2.0
		Equal resampling	33.7	47.5	30.7	15.2	0.1	0.0
		Square-root resampling	39.7	50.9	37.7	23.3	23.5	2.0

Table 18: Detailed results of applying resampling methods to the ImageNet-LT dataset.“-” means the corresponding experiment is hard to implement due to the huge amount of data.

			Mean	Many	Med.	Few	Harmonic mean	Worst case
CLIP-ViT-B/16	FFT	Baseline	49.9	69.0	44.0	16.6	0.0	0.0
		Random Over-Sampling	-	-	-	-	-	-
		Random Under-Sampling	59.2	62.1	59.0	52.2	44.6	2.0
		Equal resampling	48.6	67.8	41.9	18.0	0.0	0.0
		Square-root resampling	59.9	74.8	56.1	31.2	0.2	0.0
	PEFT	Baseline	70.6	85.5	67.6	38.8	0.1	0.0
		Random Over-Sampling	-	-	-	-	-	-
		Random Under-Sampling	75.4	78.2	75	68.4	67.6	10.0
		Equal resampling	73.6	83.2	72.2	51.1	1.0	0.0
		Square-root resampling	74.5	83.9	72.5	54.7	59.7	2.0
IN21K-ViT-B/16	FFT	Baseline	52.1	70.1	45.9	23.0	0.1	0.0
		Random Over-Sampling	-	-	-	-	-	-
		Random Under-Sampling	72.6	79.2	71.7	57.0	1.0	0.0
		Equal resampling	50.1	70.1	43.1	18.7	0.0	0.0
		Square-root resampling	68.2	80.6	64.8	44.8	1.0	0.0
	PEFT	Baseline	78.2	87.5	75.8	59.9	64.4	2.0
		Random Over-Sampling	-	-	-	-	-	-
		Random Under-Sampling	83.2	85.6	82.9	77.4	78.9	16.0
		Equal resampling	79.2	87.4	77.4	61.8	69.7	8.0
		Square-root resampling	81.0	87.3	79.5	68.6	74.1	8.0

Table 19: Detailed results of applying RUSxN to the CIFAR100-LT dataset.

			Mean	Many	Med.	Few	Harmonic mean	Worst case
CLIP-ViT-B/16	FFT	RUS	56.0	71.6	61.3	31.5	21.8	1.0
		RUSx2	58.0	81.3	62.3	25.8	0.0	0.0
		RUSx5	54.0	83.0	55.5	18.3	0.0	0.0
		RUSx10	48.8	79.1	49.5	12.8	0.0	0.0
	PEFT	RUS	77.7	82.0	80.0	69.9	73.7	25.0
		RUSx2	77.5	85.3	80.6	64.6	71.6	20.0
		RUSx5	75.6	87.2	79.7	57.4	63.4	8.0
		RUSx10	73.4	88.1	77.8	50.7	56.8	6.0
IN21K-ViT-B/16	FFT	RUS	75.7	87.9	78.1	58.6	59.6	5.0
		RUSx2	70.8	90.6	73.1	44.9	35.2	1.0
		RUSx5	66.4	90.6	69.5	34.4	26.5	1.0
		RUSx10	59.8	87.7	62.1	24.4	0.1	0.0
	PEFT	RUS	86.3	91.4	87.5	79.2	77.6	11.0
		RUSx2	84.5	92.7	86.4	72.8	71.0	8.0
		RUSx5	81.0	93.5	82.7	64.5	41.6	1.0
		RUSx10	78.2	93.4	80.2	58.3	39.5	1.0

Table 20: Detailed results of applying RUSxN to the Places-LT dataset.

			Mean	Many	Med.	Few	Harmonic mean	Worst case
CLIP-ViT-B/16	FFT	RUS	42.3	42.6	45.4	34.5	0.2	0.0
		RUSx2	41.6	46.6	45.3	24.1	24.8	1.0
		RUSx5	34.6	49.4	32.9	10.9	0.1	0.0
		RUSx10	29.0	48.3	23.3	6.6	0.0	0.0
	PEFT	RUS	50.8	49.6	52.2	49.6	35.7	1.0
		RUSx2	50.6	50.5	52.6	46.1	35.8	1.0
		RUSx5	49.1	51.5	51.4	39.2	35.5	3.0
		RUSx10	47.7	52.7	48.9	33.9	0.4	0.0
IN21K-ViT-B/16	FFT	RUS	41.2	47.6	43.3	24.6	23.4	1.0
		RUSx2	38.0	50.7	36.9	16.8	0.1	0.0
		RUSx5	31.6	49.4	26.3	10.8	0.1	0.0
		RUSx10	27.7	46.3	21.2	8.4	0.1	0.0
	PEFT	RUS	45.3	46.7	47.6	37.5	32.2	2.0
		RUSx2	43.2	48.4	44.9	29.9	29.4	3.0
		RUSx5	39.1	49.2	38.5	21.6	0.2	0.0
		RUSx10	29.0	48.3	23.3	6.6	0.0	0.0

Table 21: Detailed results of applying RUSxN to the ImageNet-LT dataset.

			Mean	Many	Med.	Few	Harmonic mean	Worst case
CLIP-ViT-B/16	FFT	RUS	59.2	62.1	59.0	52.2	44.6	2.0
		RUSx2	61.3	68.5	61.2	41.4	1.0	0.0
		RUSx5	59.0	72.8	56.0	30.6	0.2	0.0
		RUSx10	55.2	72.2	50.2	24.3	0.1	0.0
	PEFT	RUS	75.4	78.2	75.0	68.4	67.6	10.0
		RUSx2	75.9	80.0	75.5	65.9	67.9	6.0
		RUSx5	75.7	81.5	75.4	60.3	66.6	8.0
		RUSx10	75.0	82.4	74.3	56.0	62.5	4.0
IN21K-ViT-B/16	FFT	RUS	72.6	79.2	71.7	57.0	1.0	0.0
		RUSx2	71.5	80.9	69.6	51.5	58.2	2.0
		RUSx5	66.0	79.9	61.9	40.9	1.0	0.0
		RUSx10	60.5	77.2	55.7	30.7	0.2	0.0
	PEFT	RUS	83.2	85.6	82.9	77.4	78.9	16.0
		RUSx2	82.7	86.0	82.3	74.5	78.3	18.0
		RUSx5	80.6	86.7	79.3	67.8	73.7	10.0
		RUSx10	79.3	87.0	77.6	63.7	70.6	8.0

Table 22: Detailed results of applying augmentation methods to the CIFAR100-LT dataset.

			Mean	Many	Med.	Few	Harmonic mean	Worst case
CLIP-ViT-B/16	FFT	Baseline	48.7	77.9	48.1	15.4	12.2	1.0
		ColorJitter	55.0	83.2	56.3	20.7	0.1	0.0
		RandAugment	56.7	84.1	57.9	23.5	0.1	0.0
		AutoAugment	57.8	85.5	58.5	24.7	0.1	0.0
	PEFT	Baseline	71.9	90.0	75.3	46.9	57.6	9.0
		ColorJitter	71.9	90.2	75.1	46.6	56.0	7.0
		RandAugment	72.1	90.1	75.4	47.3	54.7	7.0
		AutoAugment	70.1	90.1	73.8	44.5	36.1	1.0
IN21K-ViT-B/16	FFT	Baseline	71.1	89.3	72.6	48.0	50.6	3.0
		ColorJitter	70.3	89.6	71.9	45.8	48.0	3.0
		RandAugment	70.0	89.6	70.7	46.3	45.4	2.0
		AutoAugment	71.6	90.7	72.3	48.4	54.2	7.0
	PEFT	Baseline	81.6	93.3	81.9	67.6	41.9	1.0
		ColorJitter	80.7	93.5	80.9	65.4	41.2	1.0
		RandAugment	81.5	93.7	81.5	67.2	54.7	3.0
		AutoAugment	81.3	93.3	81.8	66.7	42.2	1.0

Table 23: Detailed results of applying augmentation methods to the Places-LT dataset.

			Mean	Many	Med.	Few	Harmonic mean	Worst case
CLIP-ViT-B/16	FFT	Baseline	23.7	39.8	18.5	6.0	0.1	0.0
		ColorJitter	24.7	40.5	19.8	6.8	0.1	0.0
		RandAugment	25.4	41.6	20.4	6.9	0.1	0.0
		AutoAugment	24.9	41.8	19.8	5.6	0.0	0.0
	PEFT	Baseline	39.8	54.5	35.7	22.3	0.1	0.0
		ColorJitter	39.8	54.0	35.7	22.7	0.1	0.0
		RandAugment	40.4	54.7	36.5	23.1	0.1	0.0
		AutoAugment	40.7	54.9	36.8	23.2	0.1	0.0
IN21K-ViT-B/16	FFT	Baseline	25.7	40.9	20.5	9.4	0.1	0.0
		ColorJitter	26.0	41.4	20.9	9.5	0.1	0.0
		RandAugment	26.5	41.9	21.6	9.4	0.1	0.0
		AutoAugment	26.9	42.1	22.1	9.7	0.1	0.0
	PEFT	Baseline	31.7	45.5	27.8	15.1	0.1	0.0
		ColorJitter	32.1	45.9	28.4	15.2	0.2	0.0
		RandAugment	32.6	46.8	28.8	15.4	0.2	0.0
		AutoAugment	32.7	46.8	29.1	15.2	0.2	0.0

Table 24: Detailed results of applying augmentation methods to the ImageNet-LT dataset.

			Mean	Many	Med.	Few	Harmonic mean	Worst case
CLIP-ViT-B/16	FFT	Baseline	48.7	67.9	42.5	16.0	0.0	0.0
		ColorJitter	49.9	69.0	44.0	16.6	0.0	0.0
		RandAugment	51.0	70.2	45.1	17.6	0.0	0.0
		AutoAugment	51.8	71.3	45.9	17.0	0.0	0.0
	PEFT	Baseline	70.5	85.5	67.5	38.3	0.1	0.0
		ColorJitter	70.6	85.5	67.6	38.8	0.1	0.0
		RandAugment	70.5	85.5	67.5	38.3	0.1	0.0
		AutoAugment	70.3	81.0	67.2	38.2	0.1	0.0
IN21K-ViT-B/16	FFT	Baseline	50.8	69.1	44.4	21.8	0.1	0.0
		ColorJitter	52.1	70.1	45.9	23.0	0.1	0.0
		RandAugment	53.4	71.4	47.1	24.5	0.1	0.0
		AutoAugment	54.1	72.1	48.1	24.2	0.1	0.0
	PEFT	Baseline	78.2	87.4	76.0	59.8	1.0	0.0
		ColorJitter	78.2	87.5	75.8	59.9	64.4	2.0
		RandAugment	78.1	87.5	75.7	59.6	63.8	2.0
		AutoAugment	78.2	87.5	75.9	60.1	66.2	6.0

Table 25: Detailed results of applying different losses to the CIFAR100-LT dataset.

			Mean	Many	Med.	Few	Harmonic mean	Worst case
CLIP-ViT-B/16	FFT	CE loss	54.6	82.9	55.9	20.1	0.0	0.0
		Focal loss	52.7	81.4	53.0	19.0	17.9	1.0
		LDAM loss	53.6	78.5	52.9	25.4	0.1	0.0
		Class Balanced loss	54.7	83.4	56.1	19.4	0.1	0.0
		Generalized Re-Weight	50.9	80.4	50.9	16.5	0.0	0.0
		Balanced Softmax Loss	58.0	75.5	58.9	36.5	42.3	6.0
		Logit Adjustment loss	62.7	74.8	62.1	49.4	55.3	18.0
		LADE loss	18.2	26.3	19.9	6.9	0.0	0.0
	PEFT	CE loss	71.9	90.2	75.1	46.6	56.0	7.0
		Focal loss	71.2	89.5	74.0	46.7	58.3	10.0
		LDAM loss	73.6	89.5	77.4	50.7	0.1	0.0
		Class Balanced loss	72.5	90.2	75.3	48.6	57.7	9.0
		Generalized Re-Weight	71.8	84.0	78.3	50.1	55.8	9.0
		Balanced Softmax Loss	80.1	86.5	80.0	72.9	77.5	38.0
		Logit Adjustment loss	79.8	80.6	79.3	79.5	77.8	47.0
		LADE loss	79.9	85.7	79.0	74.1	77.1	42.0
IN21K-ViT-B/16	FFT	CE loss	70.3	89.6	71.9	45.8	48.0	3.0
		Focal loss	69.4	89.3	71.1	44.3	43.9	2.0
		LDAM loss	64.4	85.9	67.0	36.3	41.5	4.0
		Class Balanced loss	69.4	89.6	71.3	43.7	50.1	5.0
		Generalized Re-Weight	66.9	88.9	69.5	38.1	0.0	0.1
		Balanced Softmax Loss	75.8	88.7	76.4	59.9	63.0	6.0
		Logit Adjustment loss	73.1	88.4	73.1	55.1	64.7	15.0
		LADE loss	72.8	89.9	72.4	53.2	48.8	2.0
	PEFT	CE loss	80.7	93.5	80.9	65.4	41.2	1.0
		Focal loss	81.4	93.5	81.3	67.5	52.9	2.0
		LDAM loss	82.8	93.3	83.3	70.0	67.6	6.0
		Class Balanced loss	80.3	93.4	80.7	64.6	41.7	1.0
		Generalized Re-Weight	81.8	93.0	84.0	66.3	62.9	5.0
		Balanced Softmax Loss	85.1	92.0	84.8	77.4	79.5	18.0
		Logit Adjustment loss	86.3	91.9	85.9	81.3	83.2	28.0
		LADE loss	86.0	93.0	85.0	79.2	81.6	23.0

Table 26: Detailed results of applying different losses to the Places-LT dataset.

			Mean	Many	Med.	Few	Harmonic mean	Worst case
CLIP-ViT-B/16	FFT	CE loss	24.7	40.5	19.8	6.8	0.1	0.0
		Focal loss	24.3	40.5	19.2	6.3	0.1	0.0
		LDAM loss	24.7	37.9	21.2	8.6	0.0	0.0
		Class Balanced loss	25.1	40.7	20.3	7.3	0.0	0.0
		Generalized Re-Weight	22.0	38.8	16.3	4.1	0.0	0.0
		Balanced Softmax Loss	31.3	39.7	28.0	23.3	20.6	3.0
		Logit Adjustment loss	32.0	36.2	29.9	29.3	21.6	3.0
		LADE loss	16.8	23.0	16.7	5.5	0.0	0.0
	PEFT	CE loss	39.8	53.9	35.9	22.5	0.1	0.0
		Focal loss	39.0	52.9	35.1	22.1	0.2	0.0
		LDAM loss	41.1	54.7	37.4	24.3	0.0	0.0
		Class Balanced loss	40.2	54.0	35.8	24.6	0.1	0.0
		Generalized Re-Weight	44.5	51.1	46.3	28.2	0.4	0.0
		Balanced Softmax Loss	48.8	49.7	49.0	46.9	39.4	4.0
		Logit Adjustment loss	48.0	41.4	50.5	54.7	0.4	0.0
		LADE loss	49.2	49.9	49.3	47.6	35.4	1.0
IN21K-ViT-B/16	FFT	CE loss	26.0	41.4	20.9	9.5	0.1	0.0
		Focal loss	25.9	41.2	21.0	8.8	0.1	0.0
		LDAM loss	25.0	39.9	20.0	9.1	0.1	0.0
		Class Balanced loss	26.0	41.2	21.2	8.7	0.1	0.0
		Generalized Re-Weight	23.4	39.8	17.8	6.2	0.0	0.0
		Balanced Softmax Loss	30.3	41.3	26.8	18.1	16.9	2.0
		Logit Adjustment loss	31.9	40.3	29.0	23.2	20.1	2.0
		LADE loss	27.3	38.8	22.7	16.5	15.2	2.0
	PEFT	CE loss	31.9	45.8	28.2	15.0	0.2	0.0
		Focal loss	30.9	45.0	26.9	14.0	0.1	0.0
		LDAM loss	34.9	46.9	31.5	20.5	0.4	0.0
		Class Balanced loss	32.0	45.9	28.1	15.0	0.1	0.0
		Generalized Re-Weight	34.2	47.0	32.1	15.7	0.1	0.0
		Balanced Softmax Loss	38.3	45.3	36.6	29.5	26.7	3.0
		Logit Adjustment loss	39.7	42.2	39.7	35.2	29.9	4.0
		LADE loss	0.3	0.0	0.0	1.5	0.0	0.0

Table 27: Detailed results of applying different losses to the ImageNet-LT dataset.

			Mean	Many	Med.	Few	Harmonic mean	Worst case
CLIP-ViT-B/16	FFT	CE loss	49.9	69.0	44.0	16.6	0.0	0.0
		Focal loss	48.2	67.4	41.8	16.4	0.0	0.0
		LDAM loss	50.4	67.0	45.7	20.3	0.0	0.0
		Class Balanced loss	50.0	68.8	43.9	18.2	0.0	0.0
		Generalized Re-Weight	49.0	67.7	42.8	18.0	0.0	0.0
		Balanced Softmax Loss	54.6	64.8	51.0	38.2	0.3	0.0
		Logit Adjustment loss	54.0	59.8	51.5	46.5	1.0	0.0
		LADE loss	53.0	63.4	50.7	32.1	0.1	0.0
	PEFT	CE loss	70.6	85.5	67.6	38.8	0.1	0.0
		Focal loss	70.1	84.8	67.1	39.1	0.3	0.0
		LDAM loss	71.6	85.4	69.3	40.7	0.1	0.0
		Class Balanced loss	71.2	85.5	67.7	43.2	0.5	0.0
		Generalized Re-Weight	74.5	81.8	74.2	54.6	59.8	2.0
		Balanced Softmax Loss	76.7	81.2	75.4	68.5	70.2	12.0
		Logit Adjustment loss	75.6	75.0	75.7	76.7	67.9	4.0
		LADE loss	76.3	81.1	75.3	66.6	69.3	8.0
IN21K-ViT-B/16	FFT	CE loss	52.1	70.1	45.9	23.0	0.1	0.0
		Focal loss	51.0	69.1	44.5	22.6	0.1	0.0
		LDAM loss	52.2	69.6	45.8	25.2	0.1	0.0
		Class Balanced loss	52.3	70.3	46.1	23.6	0.1	0.0
		Generalized Re-Weight	50.9	69.3	44.5	21.0	0.1	0.0
		Balanced Softmax Loss	55.6	68.4	51.5	35.3	36.7	0.0
		Logit Adjustment loss	56.2	66.2	52.6	40.5	1.0	0.0
		LADE loss	48.4	61.3	43.1	30.7	0.3	0.0
	PEFT	CE loss	78.2	87.5	75.8	59.9	64.4	2.0
		Focal loss	77.4	86.9	74.7	59.7	63.9	2.0
		LDAM loss	79.4	87.2	77.3	64.9	69.5	4.0
		Class Balanced loss	78.2	87.5	75.8	60.5	64.3	2.0
		Generalized Re-Weight	78.8	87.0	77.2	61.3	66.4	4.0
		Balanced Softmax Loss	81.2	85.6	79.8	73.6	76.3	16.0
		Logit Adjustment loss	81.6	83.7	80.6	78.7	77.6	16.0
		LADE loss	81.2	86.1	79.4	74.0	76.6	16.0

Table 28: Detailed results of applying different classifiers to the CIFAR100-LT dataset.

			Mean	Many	Med.	Few	Harmonic mean	Worst case
CLIP-ViT-B/16	FFT	Linear classifier	54.6	82.9	55.9	20.1	0.0	0.0
		Cosine classifier	56.4	84.3	57.1	22.9	0.0	0.0
		τ-normalized classifier ($\tau = 0.5$)	55.6	83.5	56.8	21.6	0.1	0.0
		τ-normalized classifier ($\tau = 1$)	55.6	83.6	56.2	22.2	0.1	0.0
		τ-normalized classifier ($\tau = 2$)	54.8	83.1	55.1	21.3	0.1	0.0
	PEFT	Linear classifier	71.9	90.2	75.1	46.6	56.0	7.0
		Cosine classifier	72.2	90.2	74.5	48.5	37.9	1.0
		τ-normalized classifier ($\tau = 0.5$)	71.7	89.9	74.3	47.3	54.9	6.0
		τ-normalized classifier ($\tau = 1$)	71.9	90.0	74.6	47.6	54.1	5.0
		τ-normalized classifier ($\tau = 2$)	71.8	89.9	73.7	48.4	56.7	8.0
IN21K-ViT-B/16	FFT	Linear classifier	70.3	89.6	71.9	45.8	48.0	3.0
		Cosine classifier	69.6	90.2	70.7	44.3	31.6	1.0
		τ-normalized classifier ($\tau = 0.5$)	69.3	89.6	69.0	46.1	49.0	4.0
		τ-normalized classifier ($\tau = 1$)	68.9	89.9	70.1	42.9	48.3	4.0
		τ-normalized classifier ($\tau = 2$)	68.8	89.5	69.7	43.6	45.8	3.0
	PEFT	Linear classifier	80.7	93.5	80.9	65.4	41.2	1.0
		Cosine classifier	83.9	94.8	84.1	71.0	65.0	6.0
		τ-normalized classifier ($\tau = 0.5$)	80.8	93.3	80.6	66.2	41.7	1.0
		τ-normalized classifier ($\tau = 1$)	80.9	93.4	80.7	66.5	42.6	1.0
		τ-normalized classifier ($\tau = 2$)	81.2	93.3	81.0	67.2	58.7	3.0

Table 29: Detailed results of applying different classifiers to the Places-LT dataset.

			Mean	Many	Med.	Few	Harmonic mean	Worst case
CLIP-ViT-B/16	FFT	Linear classifier	24.9	40.7	20.1	6.8	0.0	0.0
		Cosine classifier	24.9	40.9	19.9	6.6	0.0	0.0
		τ-normalized classifier ($\tau = 0.5$)	24.7	40.9	19.8	6.2	0.0	0.0
		τ-normalized classifier ($\tau = 1$)	24.6	41.3	19.2	6.0	0.0	0.0
		τ-normalized classifier ($\tau = 2$)	23.5	40.3	17.8	5.9	0.0	0.0
	PEFT	Linear classifier	39.8	53.9	35.9	22.5	0.1	0.0
		Cosine classifier	40.6	55.2	35.9	24.2	0.2	0.0
		τ-normalized classifier ($\tau = 0.5$)	40.3	54.9	36.1	22.8	0.1	0.0
		τ-normalized classifier ($\tau = 1$)	40.0	54.7	35.4	23.4	0.2	0.0
		τ-normalized classifier ($\tau = 2$)	37.6	53.1	32.8	20.2	0.1	0.0
IN21K-ViT-B/16	FFT	Linear classifier	26.0	41.4	20.9	9.5	0.1	0.0
		Cosine classifier	27.1	43.3	21.8	9.1	0.1	0.0
		τ-normalized classifier ($\tau = 0.5$)	25.8	41.5	20.6	8.7	0.1	0.0
		τ-normalized classifier ($\tau = 1$)	25.4	41.3	20.1	8.1	0.0	0.0
		τ-normalized classifier ($\tau = 2$)	24.8	41.8	19.2	6.3	0.0	0.0
	PEFT	Linear classifier	31.9	45.8	28.2	15.0	0.2	0.0
		Cosine classifier	38.1	53.4	33.7	20.2	0.4	0.0
		τ-normalized classifier ($\tau = 0.5$)	32.1	46.4	28.2	14.7	0.1	0.0
		τ-normalized classifier ($\tau = 1$)	32.3	47.3	27.9	14.9	0.1	0.0
		τ-normalized classifier ($\tau = 2$)	32.1	47.6	27.2	14.7	0.1	0.0

Table 30: Detailed results of applying different classifiers to the ImageNet-LT dataset.

			Mean	Many	Med.	Few	Harmonic mean	Worst case
CLIP-ViT-B/16	FFT	Linear classifier	49.9	69.0	44.0	16.6	0.0	0.0
		Cosine classifier	50.0	69.6	43.7	16.8	0.1	0.0
		τ-normalized classifier ($\tau = 0.5$)	49.8	69.0	43.8	16.5	0.0	0.0
		τ-normalized classifier ($\tau = 1$)	49.0	68.5	42.7	16.2	0.0	0.0
		τ-normalized classifier ($\tau = 2$)	45.8	66.0	38.4	14.5	0.0	0.0
	PEFT	Linear classifier	70.6	85.5	67.6	38.8	0.1	0.0
		Cosine classifier	70.5	85.4	67.0	40.6	0.2	0.0
		τ-normalized classifier ($\tau = 0.5$)	70.5	85.5	67.3	39.5	0.2	0.0
		τ-normalized classifier ($\tau = 1$	70.1	85.4	66.6	39.5	0.2	0.0
		τ-normalized classifier ($\tau = 2$)	67.2	84.0	63.0	34.8	0.2	0.0
IN21K-ViT-B/16	FFT	Linear classifier	52.1	70.1	45.9	23	0.1	0.0
		Cosine classifier	54.4	72.7	48.4	23.6	0.1	0.0
		τ-normalized classifier ($\tau = 0.5$)	51.6	69.4	45.4	23	0.1	0.0
		τ-normalized classifier ($\tau = 1$)	50.5	69.1	44.1	20.1	0.1	0.0
		τ-normalized classifier ($\tau = 2$)	49.4	68.9	42.3	18.8	0.1	0.0
	PEFT	Linear classifier	78.2	87.5	75.8	59.9	64.4	2.0
		Cosine classifier	80.2	88.9	78.1	63.1	0.5	0.0
		τ-normalized classifier ($\tau = 0.5$)	76.9	86.9	74.4	57.4	61.7	2.0
		τ-normalized classifier ($\tau = 1$)	75.5	86.3	72.6	54.7	59.4	2.0
		τ-normalized classifier ($\tau = 2$)	74.6	85.5	71.3	55.4	1.0	0.0

Table 31: Detailed results of applying knowledge distillation to the CIFAR100-LT dataset.

				Mean	Many	Med.	Few	Harmonic mean	Worst case
Teacher	IN21K-ViT-B/16	PEFT		88.8	91.8	88.0	86.3	81.4	9.0
Student	DeiT-S	FFT	Baseline	67.3	88.9	67.9	41.5	29.4	1.0
			distillation	70.4	91.0	71.4	45.3	31.4	1.0
		PEFT	Baseline	69.9	89.5	70.5	46.4	0.1	0.0
			distillation	70.0	89.3	70.4	47.0	0.1	0.0
	DeiT-Ti	FFT	Baseline	58.7	84.3	60.1	27.2	26.6	2.0
			distillation	61.7	86.7	62.3	31.7	24.5	1.0
		PEFT	Baseline	60.8	84.3	61.6	32.6	0.1	0.0
			distillation	60.6	84.3	61.3	32.3	0.0	0.0

Table 32: Detailed results of applying knowledge distillation to the Places-LT dataset.

				Mean	Many	Med.	Few	Harmonic mean	Worst case
Teacher	CLIP-ViT-B/16	PEFT		51.5	50.9	52.2	50.9	37.1	1.0
Student	DeiT-S	FFT	Baseline	27.1	43.0	22.5	7.9	0.1	0.0
			distillation	30.2	46.5	25.6	10.8	0.1	0.0
		PEFT	Baseline	32.1	48.4	27.3	13.1	0.1	0.0
			distillation	32.5	49.0	27.5	13.8	0.1	0.0
	DeiT-Ti	FFT	Baseline	24.6	41.1	19.5	5.9	0.0	0.0
			distillation	28.6	45.2	23.8	9.0	0.1	0.0
		PEFT	Baseline	29.4	45.5	24.4	11.2	0.1	0.0
			distillation	30.0	46.2	25.0	11.3	0.1	0.0

Table 33: Detailed results of applying knowledge distillation to the ImageNet-LT dataset.

				Mean	Many	Med.	Few	Harmonic mean	Worst case
Teacher	IN21K-ViT-B/16	PEFT		83.6	85.8	83.0	80.0	80.1	16.0
Student	DeiT-S	FFT	Baseline	58.3	74.1	53.7	29.9	0.1	0.0
			distillation	60.5	75.8	56.2	32.6	0.2	0.0
		PEFT	Baseline	74.6	84.6	72.3	54.5	1.0	0.0
			distillation	74.9	84.6	72.6	55.9	57.6	2.0
	DeiT-Ti	FFT	Baseline	50.8	68.7	45.2	20.2	0.0	0.0
			distillation	52.7	70.3	47.2	22.4	0.1	0.0
		PEFT	Baseline	65.6	78.8	62.3	40.2	0.5	0.0
			distillation	65.9	78.9	62.6	40.5	1.0	0.0

Table 34: Detailed results of applying ensemble learning to the CIFAR100-LT dataset.

			Mean	Many	Med.	Few	Harmonic mean	Worst case
CLIP-ViT-B/16	FFT	Baseline	54.6	82.9	55.9	20.1	0.0	0.0
		Ensemble	55.6	83.7	56.4	22.0	0.1	0.0
	PEFT	Baseline	71.9	90.2	75.1	46.6	56.0	7.0
		Ensemble	76	89.4	78.8	57.1	65.7	10.0
IN21K-ViT-B/16	FFT	Baseline	70.3	89.6	71.9	45.8	48.0	3.0
		Ensemble	68.6	90.7	70.0	41.3	46.2	4.0
	PEFT	Baseline	80.7	93.5	80.9	65.4	41.2	1.0
		Ensemble	82.2	93.6	82.9	68.1	60.7	4.0

Table 35: Detailed results of applying ensemble learning to the Places-LT dataset.

			Mean	Many	Med.	Few	Harmonic mean	Worst case
CLIP-ViT-B/16	FFT	Baseline	24.9	40.7	20.1	6.8	0.0	0.0
		Ensemble	18.9	34.8	13.4	2.4	0.0	0.0
	PEFT	Baseline	39.8	53.9	35.9	22.5	0.1	0.0
		Ensemble	45.0	55.5	43.5	28.9	0.4	0.0
IN21K-ViT-B/16	FFT	Baseline	26.0	41.4	20.9	9.5	0.1	0.0
		Ensemble	26.7	43.1	21.4	8.6	0.1	0.0
	PEFT	Baseline	31.9	45.8	28.2	15.0	0.2	0.0
		Ensemble	36.4	49.2	33.6	19.2	17.3	1.0

Table 36: Detailed results of applying ensemble learning to the ImageNet-LT dataset.

			Mean	Many	Med.	Few	Harmonic mean	Worst case
CLIP-ViT-B/16	FFT	Baseline	49.9	69.0	44.0	16.6	0.0	0.0
		Ensemble	36.7	54.7	29.8	9.7	0.0	0.0
	PEFT	Baseline	70.6	85.5	67.6	38.8	0.1	0.0
		Ensemble	73.4	84.4	71.6	48.8	0.5	0.0
IN21K-ViT-B/16	FFT	Baseline	52.1	70.1	45.9	23.0	0.1	0.0
		Ensemble	54.2	71.9	48.6	24.1	0.1	0.0
	PEFT	Baseline	78.2	87.5	75.8	59.9	64.4	2.0
		Ensemble	80.4	87.9	78.7	65.1	70.3	4.0

Table 37: Detailed results of applying mixup to the CIFAR100-LT dataset.

			Mean	Many	Med.	Few	Harmonic mean	Worst case
CLIP-ViT-B/16	FFT	Baseline	51.0	70.3	51.0	30.3	36.4	7.0
		Mixup	68.7	81.9	69.7	51.9	61.1	19.0
	PEFT	Baseline	80.1	86.5	80.0	72.9	77.5	38.0
		Mixup	79.7	82.5	80.5	75.1	78.1	21.0
IN21K-ViT-B/16	FFT	Baseline	75.8	88.7	76.4	59.9	63.0	6.0
		Mixup	81.6	86.7	82.5	74.5	73.6	8.0
	PEFT	Baseline	85.1	92.0	84.8	77.4	79.5	18.0
		Mixup	86.7	89.3	86.2	84.1	84.0	29.0

Table 38: Detailed results of applying mixup to the Places-LT dataset.

			Mean	Many	Med.	Few	Harmonic mean	Worst case
CLIP-ViT-B/16	FFT	Baseline	31.3	39.7	28.0	23.3	20.6	3.0
		Mixup	35.8	41.8	34.6	27.6	25.5	3.0
	PEFT	Baseline	48.8	49.7	49.0	46.9	39.4	4.0
		Mixup	49.8	49.9	50.5	48.1	37.5	2.0
IN21K-ViT-B/16	FFT	Baseline	30.3	41.3	26.8	18.1	16.9	2.0
		Mixup	33.3	42.0	30.9	23.0	21.7	3.0
	PEFT	Baseline	38.3	45.3	36.6	29.5	26.7	3.0
		Mixup	45.0	48.1	44.9	39.8	35.2	5.0

Table 39: Detailed results of applying mixup to the ImageNet-LT dataset.

			Mean	Many	Med.	Few	Harmonic mean	Worst case
CLIP-ViT-B/16	FFT	Baseline	54.6	64.8	51.0	38.2	0.3	0.0
		Mixup	58.7	67.9	56.8	39.1	0.2	0.0
	PEFT	Baseline	76.7	81.2	75.4	68.5	70.2	12.0
		Mixup	75.2	78.9	74.8	66.2	67.3	8.0
IN21K-ViT-B/16	FFT	Baseline	55.6	68.4	51.5	35.3	36.7	0.0
		Mixup	61.5	72.0	57.6	45.6	1.0	0.0
	PEFT	Baseline	81.2	85.6	79.8	73.6	76.3	16.0
		Mixup	83.3	85.1	82.6	80.8	79.2	10.0

Table 40: Detailed results of applying label smoothing to the CIFAR100-LT dataset.

			Mean	Many	Med.	Few	Harmonic mean	Worst case
CLIP-ViT-B/16	FFT	CE	54.6	82.9	55.9	20.1	0.0	0.0
		CE (w/ LS)	56.2	85.2	56.8	21.7	15.4	1.0
		BS	58.0	75.5	58.9	36.5	42.3	6.0
		BS (w/ LS)	59.8	71.4	57.0	49.6	51.0	12.0
	PEFT	CE	71.9	90.2	75.1	46.6	56.0	7.0
		CE (w/ LS)	71.7	89.8	75.2	46.6	36.1	1.0
		BS	80.1	86.5	80.0	72.9	77.5	38.0
		BS (w/ LS)	80.6	84.1	80.1	77.2	78.5	44.0
IN21K-ViT-B/16	FFT	CE	70.3	89.6	71.9	45.8	48.0	3.0
		CE (w/ LS)	71.3	91.1	72.7	46.6	42.0	2.0
		BS	75.8	88.7	76.4	59.9	63.0	6.0
		BS (w/ LS)	78.2	90.1	76.8	65.8	71.9	23.0
	PEFT	CE	80.7	93.5	80.9	65.4	41.2	1.0
		CE (w/ LS)	82.7	94.5	82.5	69.2	61.7	4.0
		BS	85.1	92.0	84.8	77.4	79.5	18.0
		BS (w/ LS)	88.1	89.5	86.6	88.2	86.6	50.0

Table 41: Detailed results of applying label smoothing to the Places-LT dataset.

			Mean	Many	Med.	Few	Harmonic mean	Worst case
CLIP-ViT-B/16	FFT	CE	24.7	40.5	19.8	6.8	0.1	0.0
		CE (w/ LS)	25.0	40.5	19.7	8.3	0.1	0.0
		BS	31.3	39.7	28.0	23.3	20.6	3.0
		BS (w/ LS)	28.6	31.9	25.5	29.7	0.4	0.0
	PEFT	CE	39.8	53.9	35.9	22.5	0.1	0.0
		CE (w/ LS)	39.7	54.6	35.7	21.2	0.0	0.0
		BS	48.8	49.7	49.0	46.9	39.4	4.0
		BS (w/ LS)	49.4	48.9	49.7	49.4	37.9	3.0
IN21K-ViT-B/16	FFT	CE	26.0	41.4	20.9	9.5	0.1	0.0
		CE (w/ LS)	26.9	43.1	21.7	8.8	0.1	0.0
		BS	30.3	41.3	26.8	18.1	16.9	2.0
		BS (w/ LS)	32.4	38.7	29.4	27.5	0.4	0.0
	PEFT	CE	31.9	45.8	28.2	15.0	0.2	0.0
		CE (w/ LS)	34.1	48.3	30.0	17.3	0.1	0.0
		BS	38.3	45.3	36.6	29.5	26.7	3.0
		BS (w/ LS)	41.8	44.6	41.2	37.8	30.6	5.0

Table 42: Detailed results of applying label smoothing to the ImageNet-LT dataset.

			Mean	Many	Med.	Few	Harmonic mean	Worst case
CLIP-ViT-B/16	FFT	CE	49.9	69.0	44.0	16.6	0.0	0.0
		CE (w/ LS)	51.4	69.7	45.8	19.1	0.0	0.0
		BS	54.6	64.8	51.0	38.2	0.3	0
		BS (w/ LS)	55.5	63.2	52.2	45.3	41.0	4.0
	PEFT	CE	70.6	85.5	67.6	38.8	0.1	0.0
		CE (w/ LS)	70.5	85.7	67.7	37.5	0.1	0.0
		BS	76.7	81.2	75.4	68.5	70.2	12.0
		BS (w/ LS)	76.7	80.1	75.7	70.3	70.5	12.0
IN21K-ViT-B/16	FFT	CE	52.1	70.1	45.9	23.0	0.1	0.0
		CE (w/ LS)	54.5	73.2	48.2	24.2	0.1	0.0
		BS	55.6	68.4	51.5	35.3	36.7	0.0
		BS (w/ LS)	59.0	68.9	54.5	43.8	43.4	2.0
	PEFT	CE	78.2	87.5	75.8	59.9	64.4	2.0
		CE (w/ LS)	80.4	88.3	78.3	65.4	66.4	2.0
		BS	81.2	85.6	79.8	73.6	76.3	16.0
		BS (w/ LS)	83.0	85.0	82.1	80.3	79.1	16.0

Table 43: Ablation experiment on CIFAR100-LT.

		Cosine Classifier	Square-root sampling	Balanced Softmax	Label Smoothing	Auto Augment	Mixup	Mean	Many	Med.	Few	Hmean	Worst
CLIP -ViT -B/16	FFT							46.9	75.6	46.3	14.1	10.7	1.0
		✓						41.5	70.6	39.1	10.2	0.0	0.0
		✓	✓					60.0	82.7	64.5	28.2	20.6	1.0
		✓	✓	✓				65.7	80.3	69.1	44.7	51.0	6.0
		✓	✓	✓	✓			67.4	80.8	70.3	48.6	55.5	8.0
		✓	✓	✓	✓	✓		29.7	38.9	31.8	16.4	0.0	0.0
		✓	✓	✓	✓		✓	49.6	61.5	52.6	32.3	25.2	1.0
		✓	✓	✓	✓	✓	✓	14.4	15.3	17.2	10.0	0.0	0.0
	PEFT							71.9	90.1	75.2	47.0	56.5	8.0
		✓						72.8	90.2	75.5	49.2	56.2	5.0
		✓	✓					77.0	87.7	78.9	62.3	68.7	11.0
		✓	✓	✓				80.1	84.5	81.0	74.0	77.0	28.0
		✓	✓	✓	✓			80.5	84.1	81.1	75.7	77.9	35.0
		✓	✓	✓	✓	✓		79.3	80.9	80.2	76.4	76.4	35.0
		✓	✓	✓	✓		✓	79.3	81.2	80.1	76.2	74.5	17.0
		✓	✓	✓	✓	✓	✓	77.5	79.3	78.1	74.9	73.1	28.0
IN21K -ViT -B/16	FFT							71.1	89.3	72.6	48.0	50.6	3.0
		✓						71.4	91.0	73.0	46.8	39.0	2.0
		✓	✓					75.1	91.4	76.6	54.3	53.3	3.0
		✓	✓	✓				82.7	90.6	83.1	72.9	74.4	9.0
		✓	✓	✓	✓			81.5	91.7	81.3	69.8	75.6	16.0
		✓	✓	✓	✓	✓		82.2	91.5	82.9	70.3	76.8	23.0
		✓	✓	✓	✓		✓	83.9	91.2	83.7	75.7	77.8	15.0
		✓	✓	✓	✓	✓	✓	84.7	89.5	85.3	78.4	81.6	26.0
	PEFT							81.6	93.3	81.9	67.6	41.9	1.0
		✓						84.2	94.9	84.1	71.8	62.0	4.0
		✓	✓					87.2	94.2	87.1	79.2	79.2	12.0
		✓	✓	✓				89.1	92.6	88.5	85.8	86.5	28.0
		✓	✓	✓	✓			89.2	91.7	88.4	87.2	87.3	40.0
		✓	✓	✓	✓	✓		88.9	90.8	88.2	87.5	87.3	43.0
		✓	✓	✓	✓		✓	88.1	89.6	88.0	86.5	84.4	19.0
		✓	✓	✓	✓	✓	✓	87.6	88.9	87.1	86.6	84.6	24.0

Table 44: Ablation experiment on Places-LT.

		Cosine Classifier	Square-root sampling	Balanced Softmax	Label Smoothing	Auto Augment	Mixup	Mean	Many	Med.	Few	Hmean	Worst
CLIP -ViT -B/16	FFT							23.7	39.8	18.5	6.0	0.1	0.0
		✓						24.5	41.0	19.2	6.3	0.0	0.0
		✓	✓					36.9	50.9	34.4	16.7	18.7	1.0
		✓	✓	✓				42.1	17.4	42.8	31.1	31.7	4.0
		✓	✓	✓	✓			42.2	49.2	42.5	28.6	31.3	5.0
		✓	✓	✓	✓	✓		43.7	47.3	45.3	33.3	32.0	4.0
		✓	✓	✓	✓		✓	45.6	48.0	47.1	37.7	30.8	1.0
		✓	✓	✓	✓	✓	✓	45.4	46.4	47.1	39.4	32.4	5.0
	PEFT							39.8	54.5	35.7	22.3	0.1	0.0
		✓						40.6	55.1	36.2	24.0	0.1	0.0
		✓	✓					48.0	56.1	46.0	37.7	31.8	1.0
		✓	✓	✓				51.3	51.3	51.9	49.9	40.4	3.0
		✓	✓	✓	✓			51.2	51.2	51.9	49.8	39.0	2.0
		✓	✓	✓	✓	✓		51.1	50.6	51.9	50.1	38.8	2.0
		✓	✓	✓	✓		✓	50.7	50.6	51.3	49.6	39.1	4.0
		✓	✓	✓	✓	✓	✓	50.2	49.9	50.9	48.9	35.8	2.0
IN21K -ViT -B/16	FFT							25.7	40.9	20.5	9.4	0.1	0.0
		✓						26.6	42.9	21.3	8.4	0.2	0.0
		✓	✓					38.2	51.9	34.8	21.0	19.3	2.0
		✓	✓	✓				42.3	50.3	41.1	30.0	30.1	4.0
		✓	✓	✓	✓			42.5	51.1	41.5	29.2	29.6	3.0
		✓	✓	✓	✓	✓		43.8	50.5	43.9	31.1	31.8	3.0
		✓	✓	✓	✓		✓	45.4	50.4	46.0	34.9	33.2	3.0
		✓	✓	✓	✓	✓	✓	46.0	49.9	47.0	36.6	33.4	3.0
	PEFT							31.7	45.5	27.8	15.1	0.1	0.0
		✓						37.8	53.5	33.5	18.9	0.1	0.0
		✓	✓					44.7	53.4	42.8	32.9	29.8	4.0
		✓	✓	✓				48.4	49.4	49.6	43.7	36.7	4.0
		✓	✓	✓	✓			47.9	49.0	49.1	43.1	36.0	4.0
		✓	✓	✓	✓	✓		48.2	49.3	49.3	43.5	36.6	5.0
		✓	✓	✓	✓		✓	48.4	48.3	49.4	46.0	34.0	1.0
		✓	✓	✓	✓	✓	✓	48.3	47.7	49.6	46.2	34.9	2.0

Table 45: Ablation experiment on ImageNet-LT.

		Cosine Classifier	Square-root sampling	Balanced Softmax	Label Smoothing	Auto Augment	Mixup	Mean	Many	Med.	Few	Hmean	Worst
CLIP -ViT -B/16	FFT							48.7	67.9	42.5	16.0	0.0	0.0
		✓						48.7	68.6	42.2	15.5	0.0	0.0
		✓	✓					60.1	75.0	56.0	32.1	0.1	0.0
		✓	✓	✓				63.2	71.9	60.9	46.6	1.0	0.0
		✓	✓	✓	✓			64.1	73.1	61.6	47.4	51.2	4.0
		✓	✓	✓	✓	✓		64.5	71.4	63.0	50.1	51.9	2.0
		✓	✓	✓	✓		✓	65.7	72.0	64.2	53.2	54.6	6.0
		✓	✓	✓	✓	✓	✓	63.9	70.0	62.7	51.0	50.1	2.0
	PEFT							70.5	85.5	67.5	38.3	0.1	0.0
		✓						70.4	85.5	67.0	39.9	0.1	0.0
		✓	✓					74.7	84.0	72.7	55.4	60.8	4.0
		✓	✓	✓				77.0	80.8	75.9	69.6	71.1	14.0
		✓	✓	✓	✓			77.2	80.5	76.3	71.5	71.2	14.0
		✓	✓	✓	✓	✓		76.6	79.3	75.9	71.2	69.8	6.0
		✓	✓	✓	✓		✓	75.5	78.3	74.6	70.4	68.1	8.0
		✓	✓	✓	✓	✓	✓	74.9	77.3	74.4	69.8	66.6	6.0
IN21K -ViT -B/16	FFT							50.8	69.1	44.4	21.8	0.1	0.0
		✓						53.1	71.4	46.9	23.0	0.1	0.0
		✓	✓					71.5	82.3	68.5	51.5	55.8	2.0
		✓	✓	✓				73.4	81.3	71.0	59.3	65.5	6.0
		✓	✓	✓	✓			75.2	82.1	73.1	62.8	67.7	10.0
		✓	✓	✓	✓	✓		75.5	81.9	74.0	62.8	68.4	10.0
		✓	✓	✓	✓		✓	76.4	82.1	74.8	65.7	69.8	10.0
		✓	✓	✓	✓	✓	✓	77.0	82.1	75.7	67.1	70.8	10.0
	PEFT							78.2	87.4	76.0	59.8	1.0	0.0
		✓						80.3	88.8	78.2	63.6	0.5	0.0
		✓	✓					82.6	88.1	81.3	71.5	75.1	6.0
		✓	✓	✓				83.6	86.4	83.0	78.2	79.6	10.0
		✓	✓	✓	✓			84.1	85.8	83.6	80.6	80.2	16.0
		✓	✓	✓	✓	✓		84.1	85.8	83.6	80.9	80.2	14.0
		✓	✓	✓	✓		✓	84.1	85.1	83.8	82.8	80.1	12.0
		✓	✓	✓	✓	✓	✓	84.2	85.1	83.9	82.8	80.3	14.0

Table 46: Ablation experiment on iNaturalist 2018.

		Cosine Classifier	Square-root sampling	Balanced Softmax	Label Smoothing	Auto Augment	Mixup	Mean	Many	Med.	Few	Hmean	Worst
CLIP -ViT -B/16	FFT							58.4	73.6	62.6	49.1	0.0	0.0
		✓						63.3	72.2	64.6	59.5	0.0	0.0
		✓	✓					68.4	70.3	69.4	66.7	0.0	0.0
		✓	✓	✓				70.9	66.1	71.3	71.5	0.0	0.0
		✓	✓	✓	✓			71.5	65.1	71.9	72.7	0.0	0.0
		✓	✓	✓	✓	✓		69.6	61.3	69.9	71.4	0.0	0.0
		✓	✓	✓	✓		✓	69.4	59.9	69.6	71.6	0.0	0.0
		✓	✓	✓	✓	✓	✓	48.7	34.2	47.2	54.4	0.0	0.0
	PEFT							69.5	82.1	73.1	61.7	0.0	0.0
		✓						75.3	81.6	76.0	72.7	0.0	0.0
		✓	✓					76.8	78.6	77.4	75.5	0.0	0.0
		✓	✓	✓				79.3	73.5	79.1	81.0	0.0	0.0
		✓	✓	✓	✓			79.0	73.0	78.9	80.6	0.0	0.0
		✓	✓	✓	✓	✓		78.3	72.0	78.4	79.8	0.0	0.0
		✓	✓	✓	✓		✓	76.9	69.1	77.0	78.8	0.0	0.0
		✓	✓	✓	✓	✓	✓	74.6	66.3	74.4	76.9	0.0	0.0
IN21K -ViT -B/16	FFT							57.8	65.3	59.1	54.2	0.0	0.0
		✓						61.5	70.3	62.9	57.5	0.0	0.0
		✓	✓					72.3	75.0	73.4	70.1	0.0	0.0
		✓	✓	✓				75.0	70.0	75.7	75.4	0.0	0.0
		✓	✓	✓	✓			74.6	69.8	75.1	75.2	0.0	0.0
		✓	✓	✓	✓	✓		74.9	68.8	75.5	75.7	0.0	0.0
		✓	✓	✓	✓		✓	73.3	65.7	73.9	74.6	0.0	0.0
		✓	✓	✓	✓	✓	✓	72.3	63.5	72.9	73.9	0.0	0.0
	PEFT							73.6	79.2	75.8	69.5	0.0	0.0
		✓						75.6	81.2	77.2	72.2	0.0	0.0
		✓	✓					79.0	80.6	80.2	77.1	0.0	0.0
		✓	✓	✓				81.1	75.6	81.7	81.9	0.1	0.0
		✓	✓	✓	✓			81.1	75.8	81.8	81.7	0.1	0.0
		✓	✓	✓	✓	✓		81.1	74.6	81.8	81.8	0.1	0.0
		✓	✓	✓	✓		✓	79.9	71.9	80.4	81.4	0.0	0.0
		✓	✓	✓	✓	✓	✓	79.4	71.2	79.9	80.8	0.0	0.0

Table 47: Comparison of LIFT and our method on accuracy and training cost. ”S/E” represents the number of training samples in each epoch, and ”Samples” represents the total number of training samples.

Datasets		Acc	Epochs	S/E	Samples
CIFAR100-IR100	LIFT	80.3	10	10.8K	108K
	Ours	**80.5**	50	1.9K	**95K**(↓)
Places-LT	LIFT	**51.5**	10	62.5K	625K
	Ours	51.2	50	8.2K	**410K**(↓)
ImageNet-LT	LIFT	77.0	10	117.0K	1.17M
	Ours	**77.2**	50	20.7K	**1.03M**(↓)
iNaturalist 2018	LIFT	**79.1**	20	437.5K	8.75M
	Ours	79.0	100	65.0K	**6.5M**(↓)

Table 48: Accuracy of our method with DINO.

Datasets	Overall	Many	Med.	Few
CIFAR100-IR100	80.3	85.1	81.7	73.0
Places-LT	43.9	45.5	45.4	37.3
ImageNet-LT	73.5	77.6	72.8	64.0